# Supplementary Material for The Emissions Model Intercomparison Project (Emissions-MIP): quantifying model sensitivity to emission characteristics

**Hamza Ahsan[1], Hailong Wang[2], Jingbo Wu[3], Mingxuan Wu[2], Steven J. Smith[1], Susanne Bauer[3], Harrison Suchyta[1], Dirk Olivié[4], Gunnar Myhre[5], Hitoshi Matsui[6], Huisheng Bian[7], Jean-François Lamarque[8], Ken Carslaw[9], Larry Horowitz[10], Leighton Regayre[9,11,12], Mian Chin[7], Michael Schulz[4], Ragnhild Bieltvedt Skeie[5], Toshihiko Takemura[13], Vaishali Naik[10]**

[1]Joint Global Change Research Institute, Pacific Northwest National Laboratory, College Park, MD, USA
[2]Atmospheric, Climate, and Earth Sciences Division, Pacific Northwest National Laboratory, Richland, WA, USA
[3]NASA Goddard Institute for Space Studies, New York, NY, USA
[4]Norwegian Meteorological Institute, Oslo, Norway
[5]CICERO Center for International Climate Research, Oslo, Norway
[6]Graduate School of Environmental Studies, Nagoya University, Nagoya, Japan
[7]NASA Goddard Space Flight Center, Greenbelt, MD, USA
[8]Climate and Global Dynamics Laboratory, National Center for Atmospheric Research, Boulder, CO, USA
[9]Institute for Climate and Atmospheric Science, School of Earth and Environment, University of Leeds, Leeds, UK
[10]NOAA Geophysical Fluid Dynamics Laboratory, Princeton, NJ, USA
[11]Met Office Hadley Centre, Exeter, Fitzroy Road, Exeter, Devon, UK
[12]Centre for Environmental Modelling and Computation, School of Earth and Environment, University of Leeds, Leeds, UK
[13]Research Institute for Applied Mechanics, Kyushu University, Fukuoka, Japan

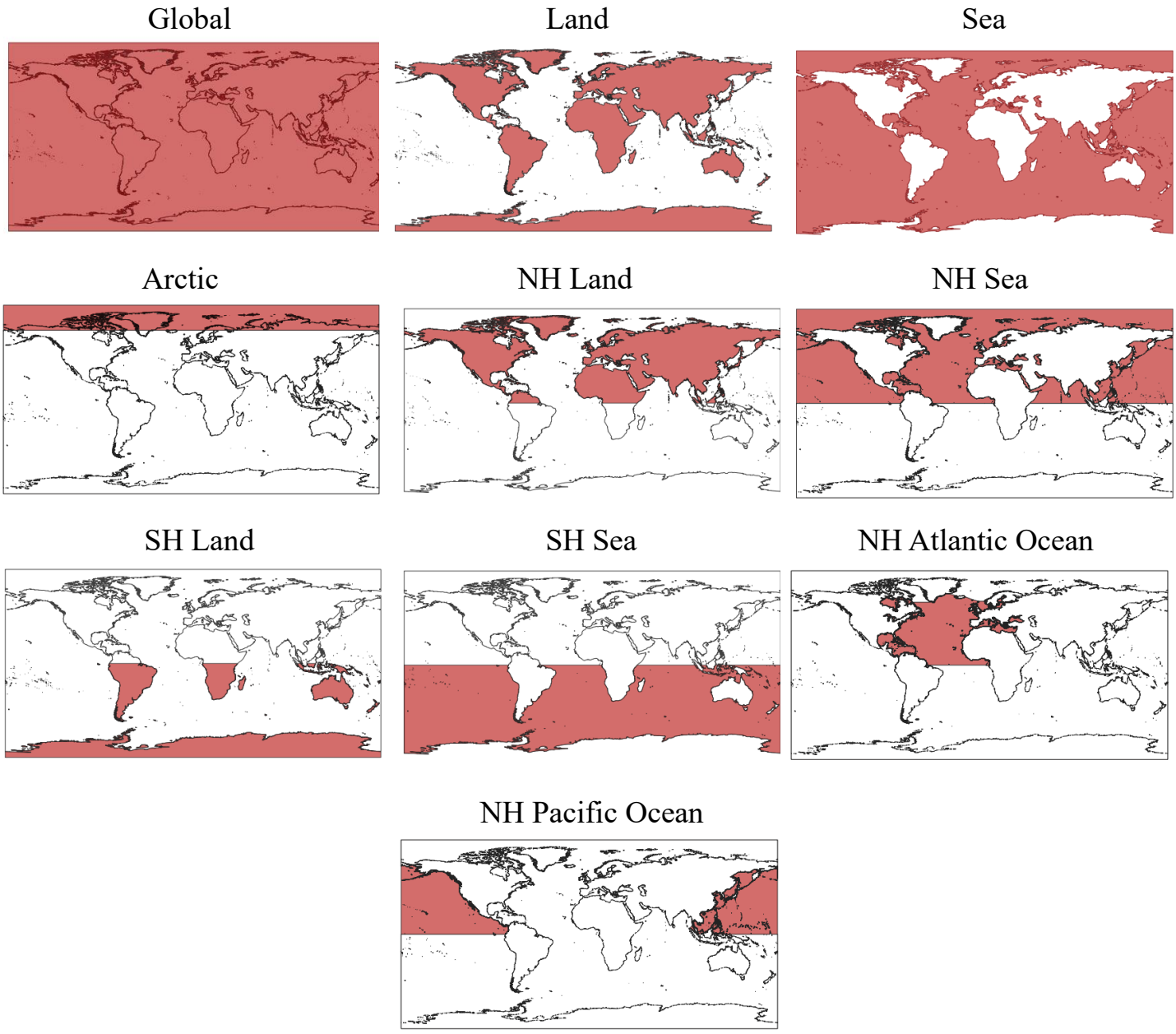


Figure S1: Global maps showing the various regions shaded in red for which diagnostics were calculated using ESMValTool.

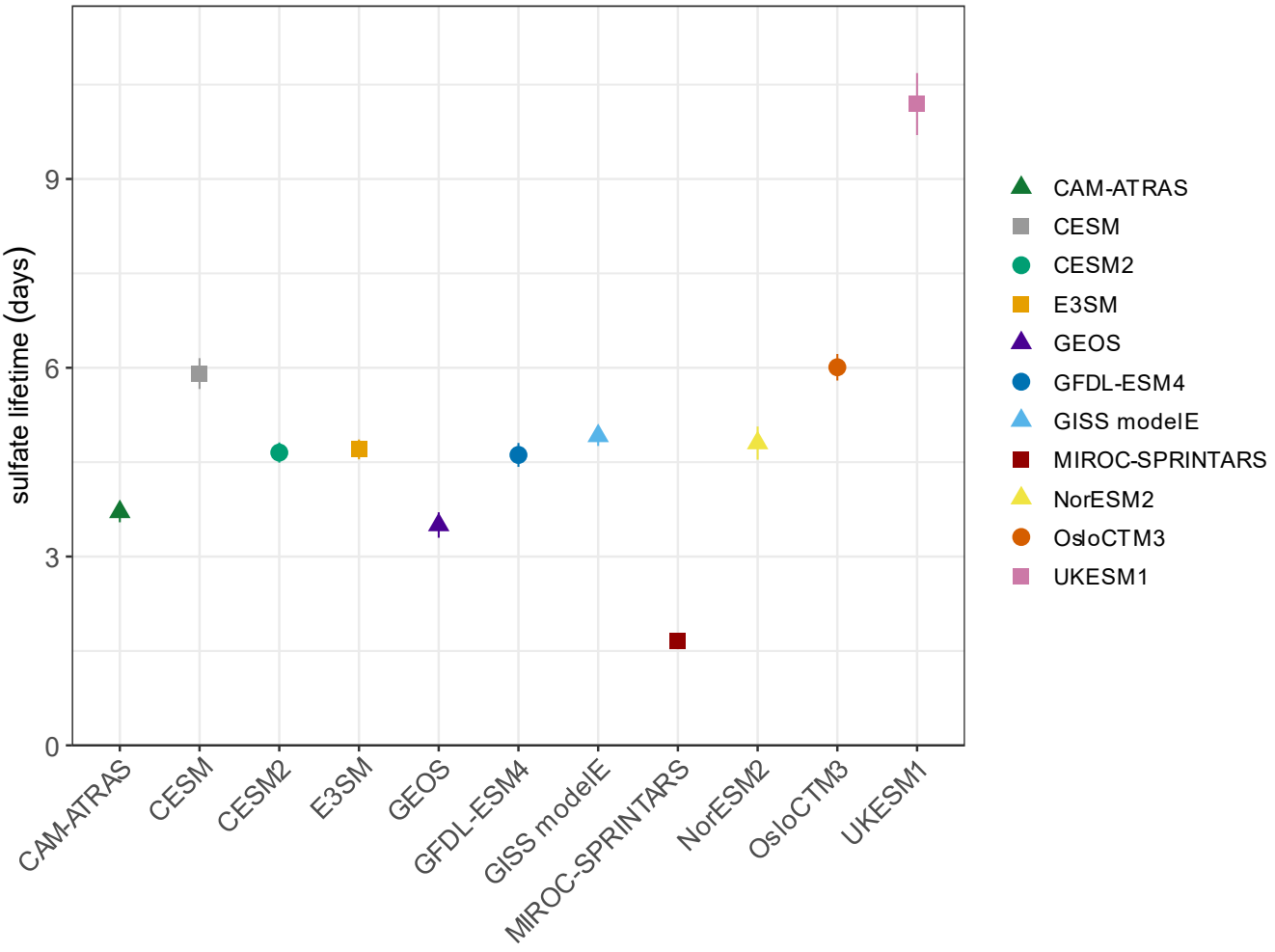


Figure S2: Northern Hemisphere land sulfate lifetime of the reference case model simulations. All results are averaged over the years 2000 – 2004, except NorESM2 is averaged over 2001 – 2005. The error bars represent interannual variability (± 1 σ).

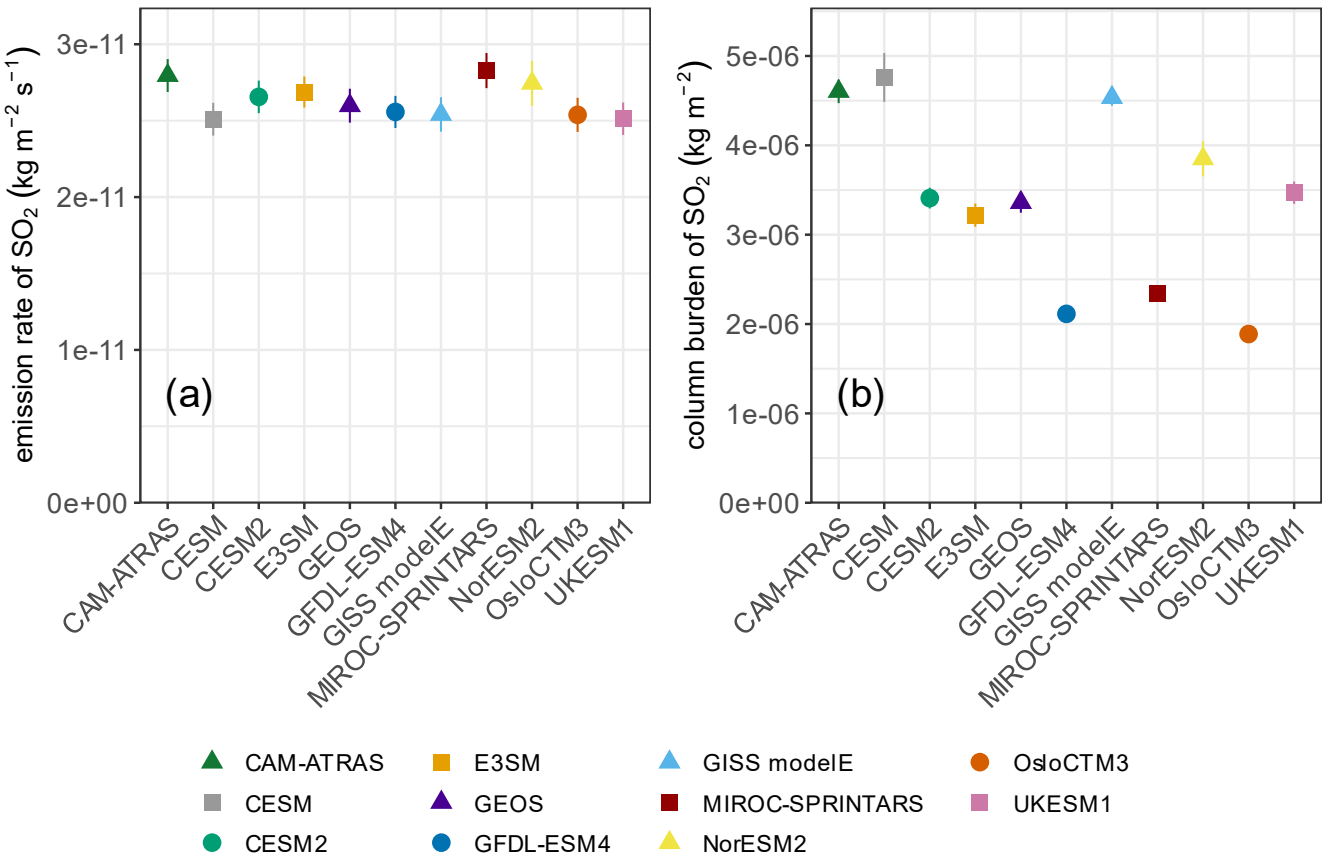


Figure S3: (a) Northern Hemisphere land $SO_2$ emission rate and (b) $SO_2$ column burden of the reference case model simulations. All results are averaged over the years 2000 – 2004, except NorESM2 is averaged over 2001 – 2005. The error bars represent interannual variability (± 1 σ).

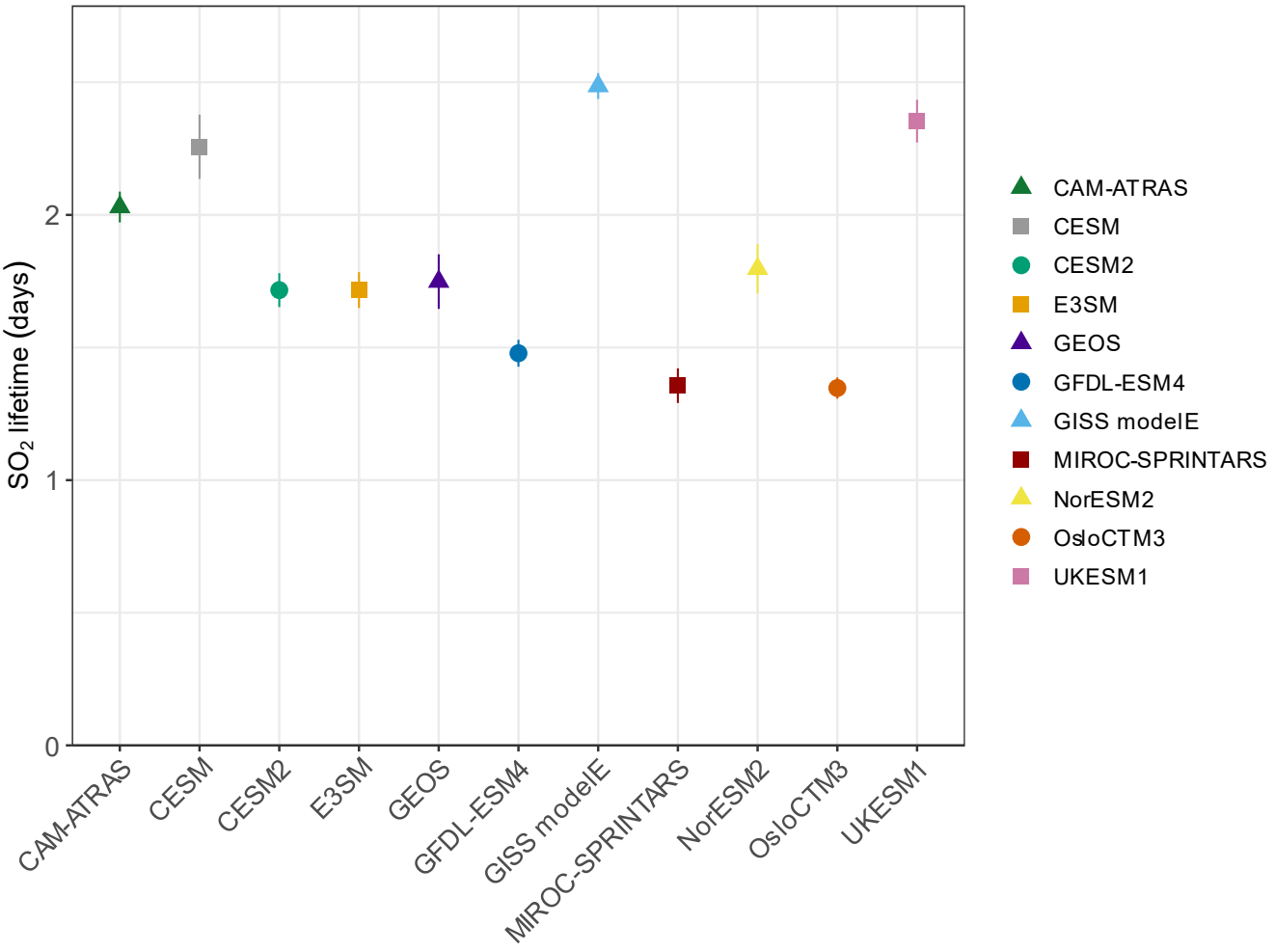


Figure S4: Global $SO_2$ lifetime of the reference case model simulations. All results are averaged over the years 2000 – 2004, except NorESM2 is averaged over 2001 – 2005. The error bars represent interannual variability (± 1 σ).

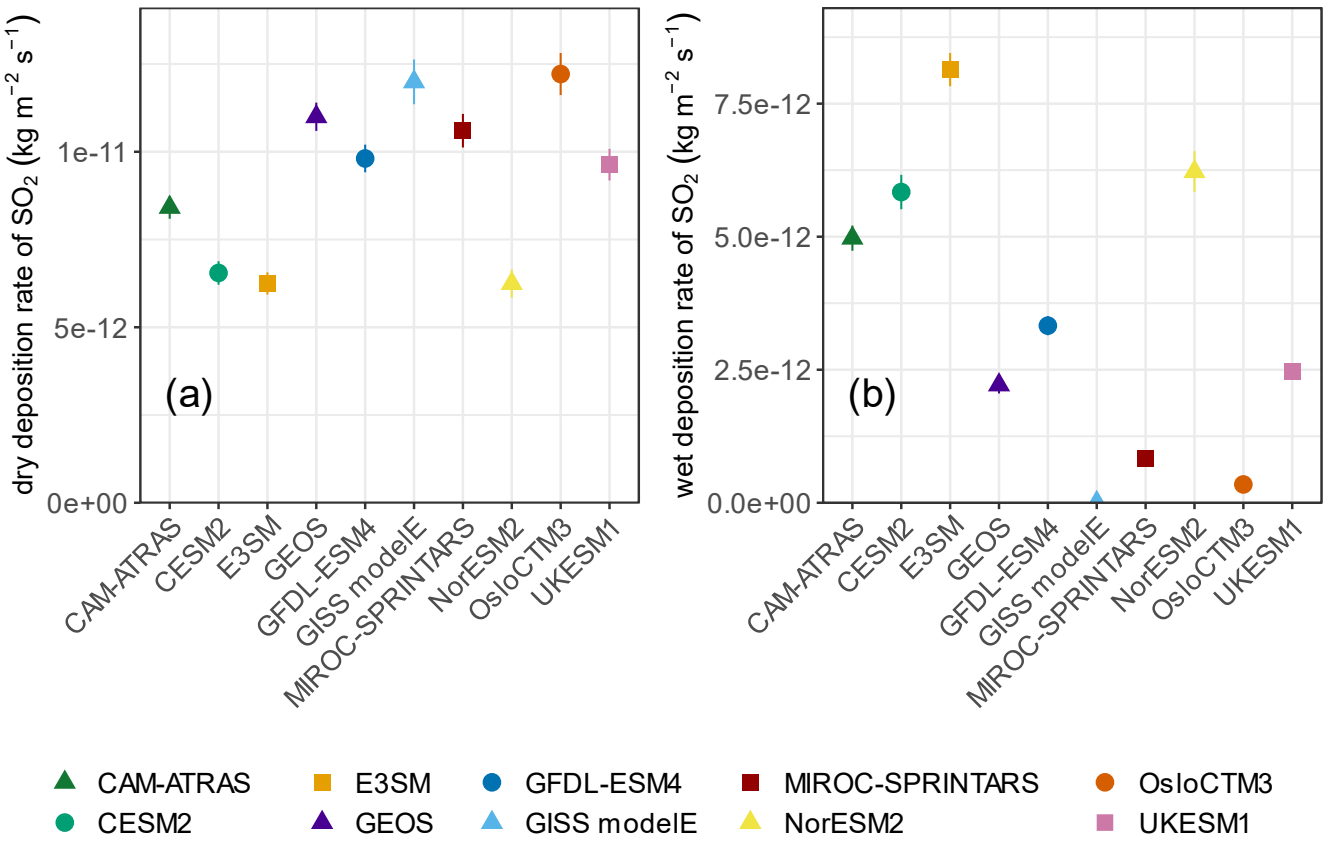


Figure S5: (a) Northern Hemisphere land dry $SO_2$ deposition rate and (b) wet $SO_2$ deposition rate of the reference case model simulations. All results are averaged over the years 2000 – 2004, except NorESM2 is averaged over 2001 – 2005. The error bars represent interannual variability (± 1 σ).

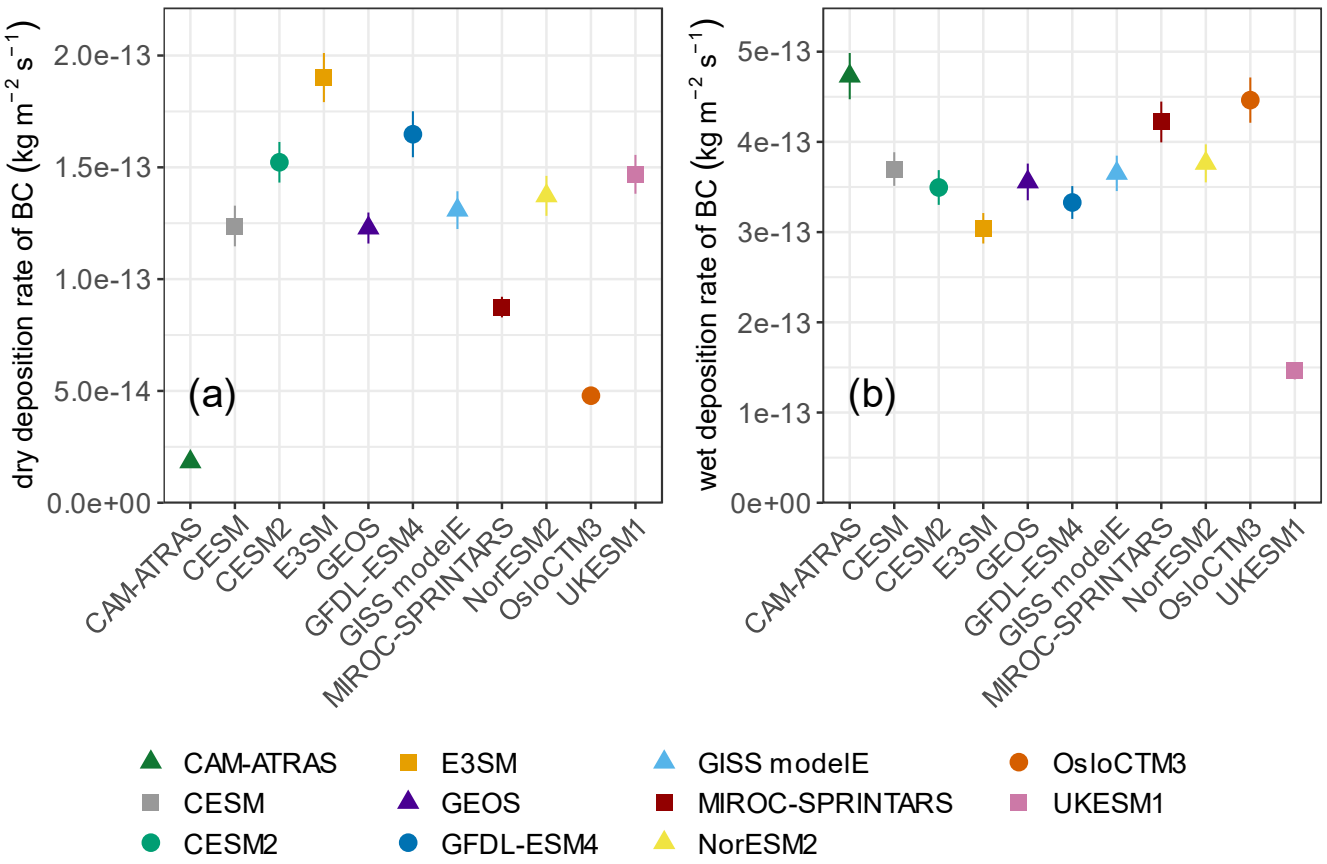


Figure S6: (a) Global dry BC deposition rate and (b) wet BC deposition rate of the reference case model simulations. All results are averaged over the years 2000 – 2004, except NorESM2 is averaged over 2001 – 2005. The error bars represent interannual variability (± 1 σ).

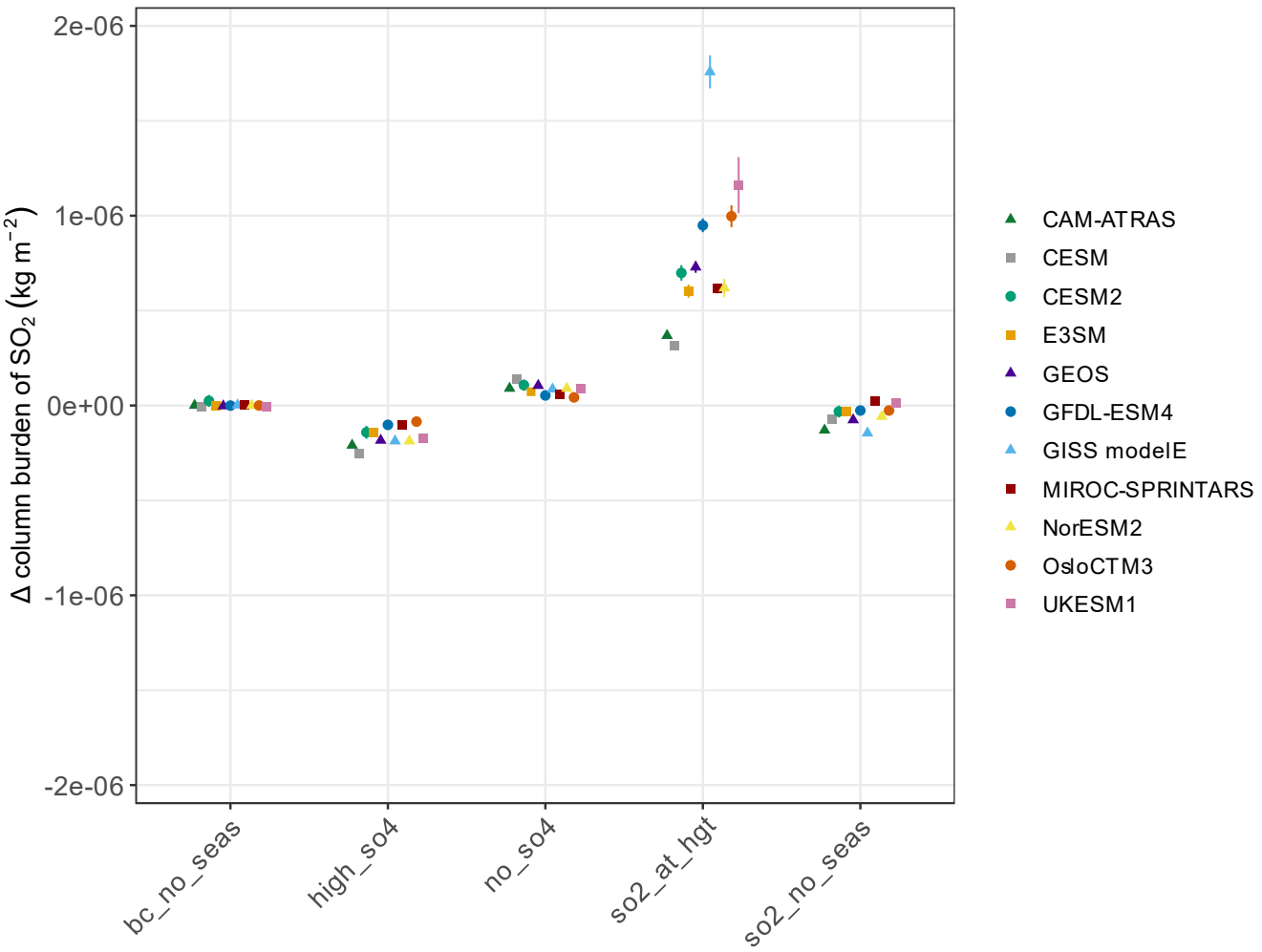


Figure S7: Absolute difference of Northern Hemisphere land $SO_2$ column burden for each perturbation. All results are averaged over the years 2000 – 2004, except NorESM2 is averaged over 2001 – 2005. The uncertainty bars represent interannual variability (± 1 σ).

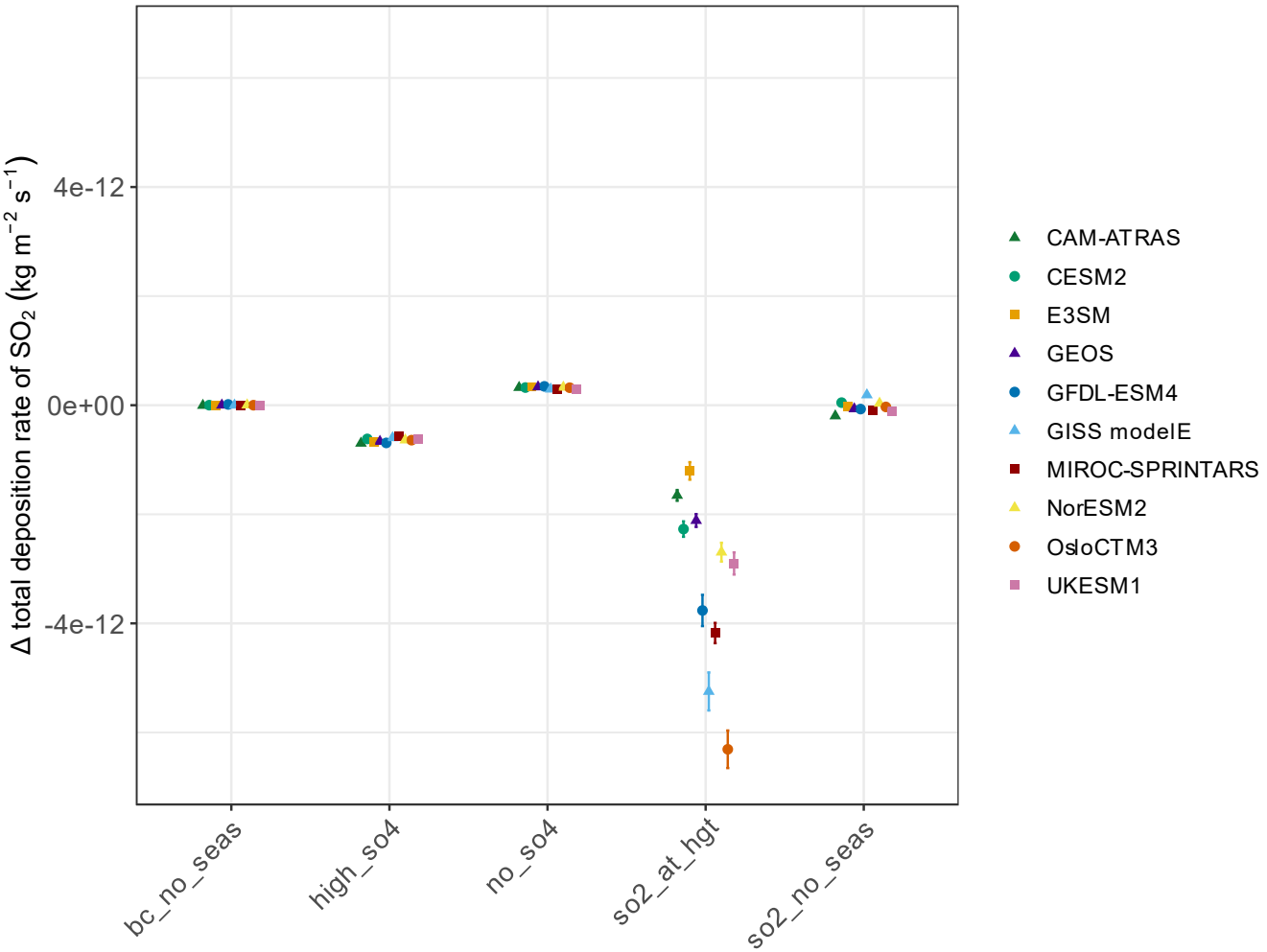


Figure S8: Absolute difference of Northern Hemisphere land total $SO_2$ deposition rate for each perturbation. All results are averaged over the years 2000 – 2004, except NorESM2 is averaged over 2001 – 2005. The uncertainty bars represent interannual variability (± 1 σ).

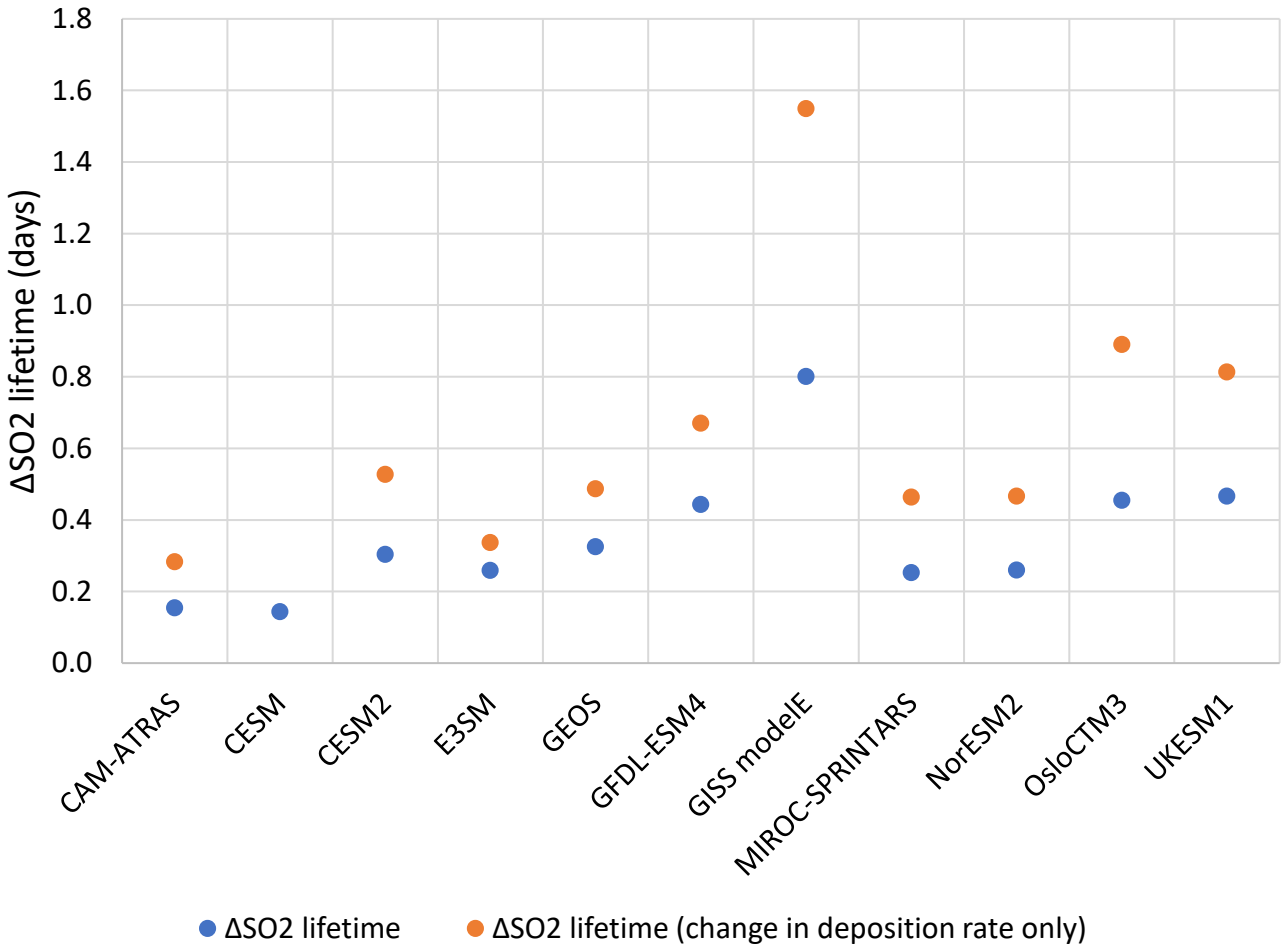


Figure S9: Absolute difference (emission at height – reference) of Northern Hemisphere land $SO_2$ lifetime, showing the relative impact of deposition vs chemical conversion. All results are averaged over the years 2000 – 2004, except NorESM2 is averaged over 2001 – 2005.

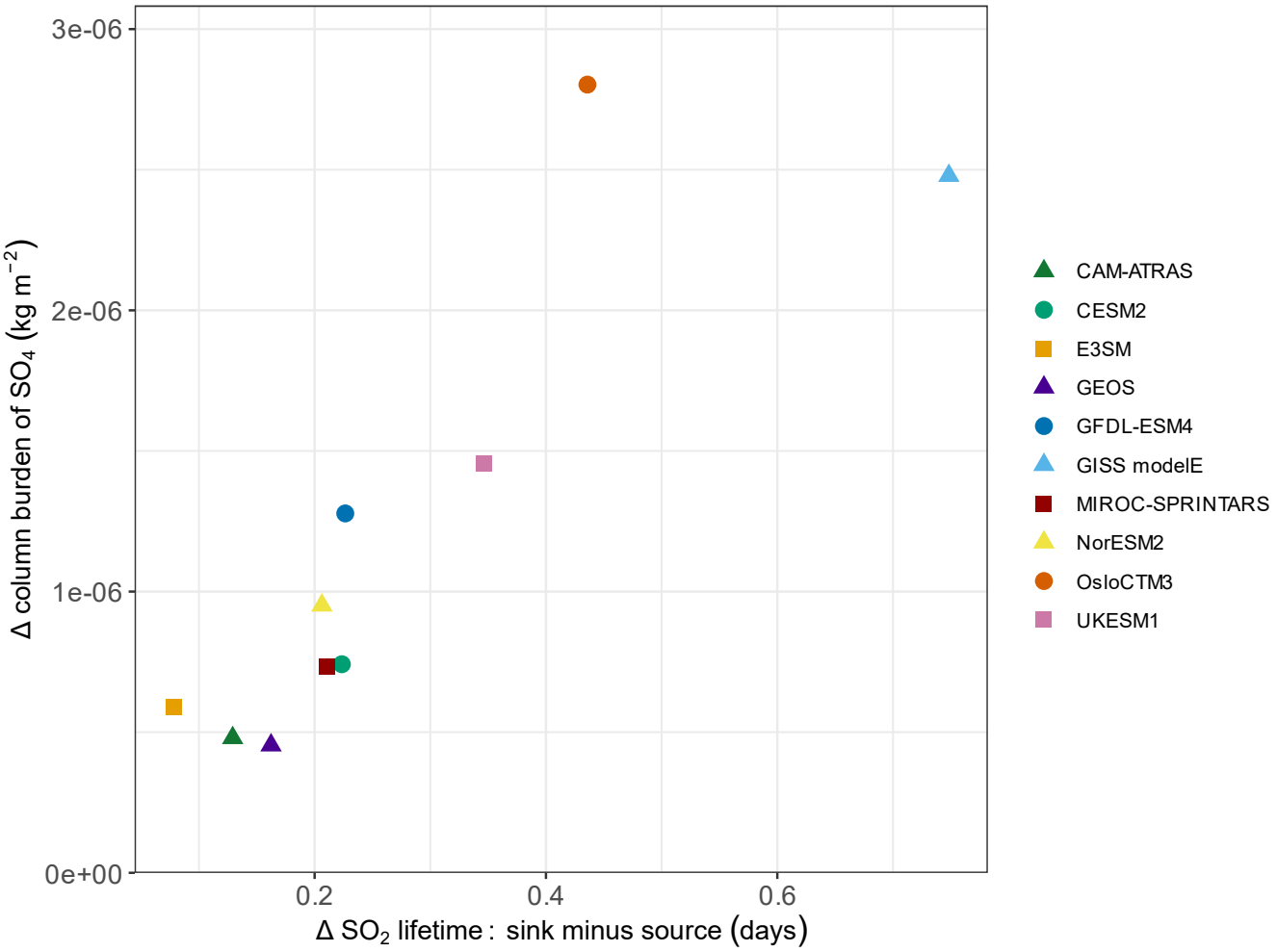


Figure S10: Absolute difference (emission at height – reference) of Northern Hemisphere land sulfate column burden vs $SO_2$ lifetime offset (sink minus source). All results are averaged over the years 2000 – 2004, except NorESM2 is averaged over 2001 – 2005.

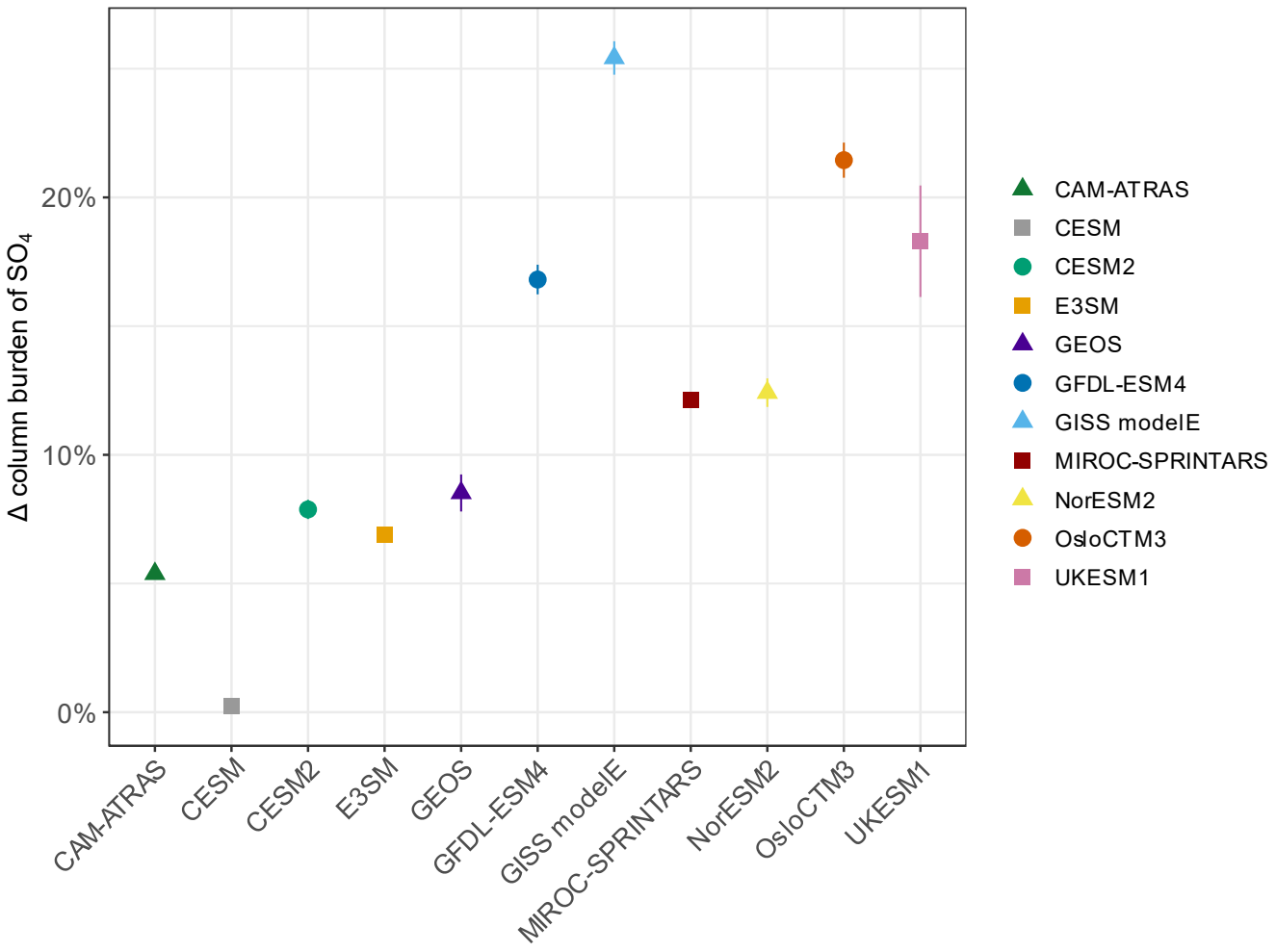


Figure S11: Percent difference (emission at height – reference) of global mean sulfate column burden. All results are averaged over the years 2000 – 2004, except NorESM2 is averaged over 2001 – 2005. The uncertainty bars represent interannual variability (± 1 σ).

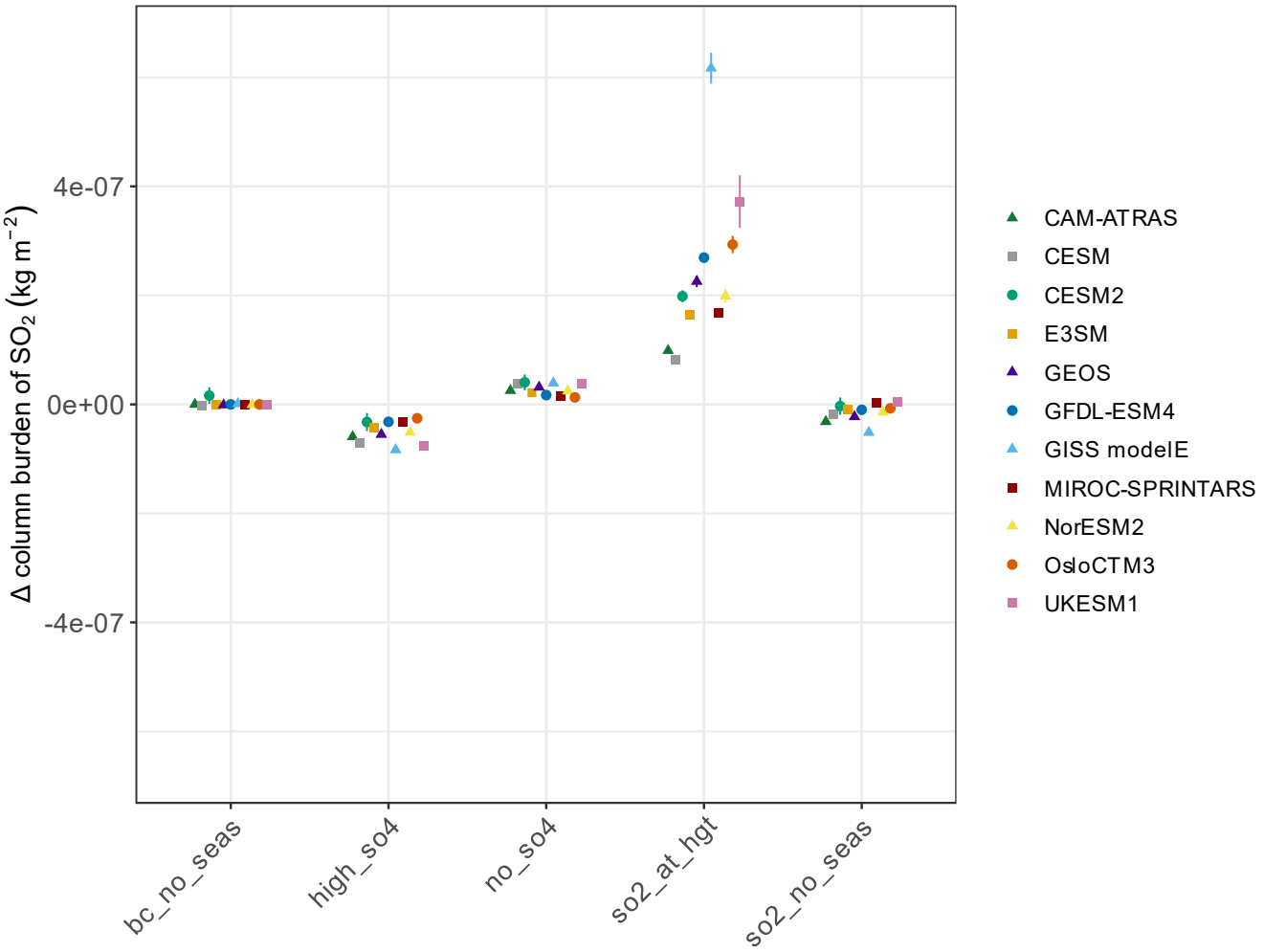


Figure S12: Absolute difference of global mean $SO_2$ column burden for each perturbation. All results are averaged over the years 2000 – 2004, except NorESM2 is averaged over 2001 – 2005. The uncertainty bars represent interannual variability (± 1 σ).

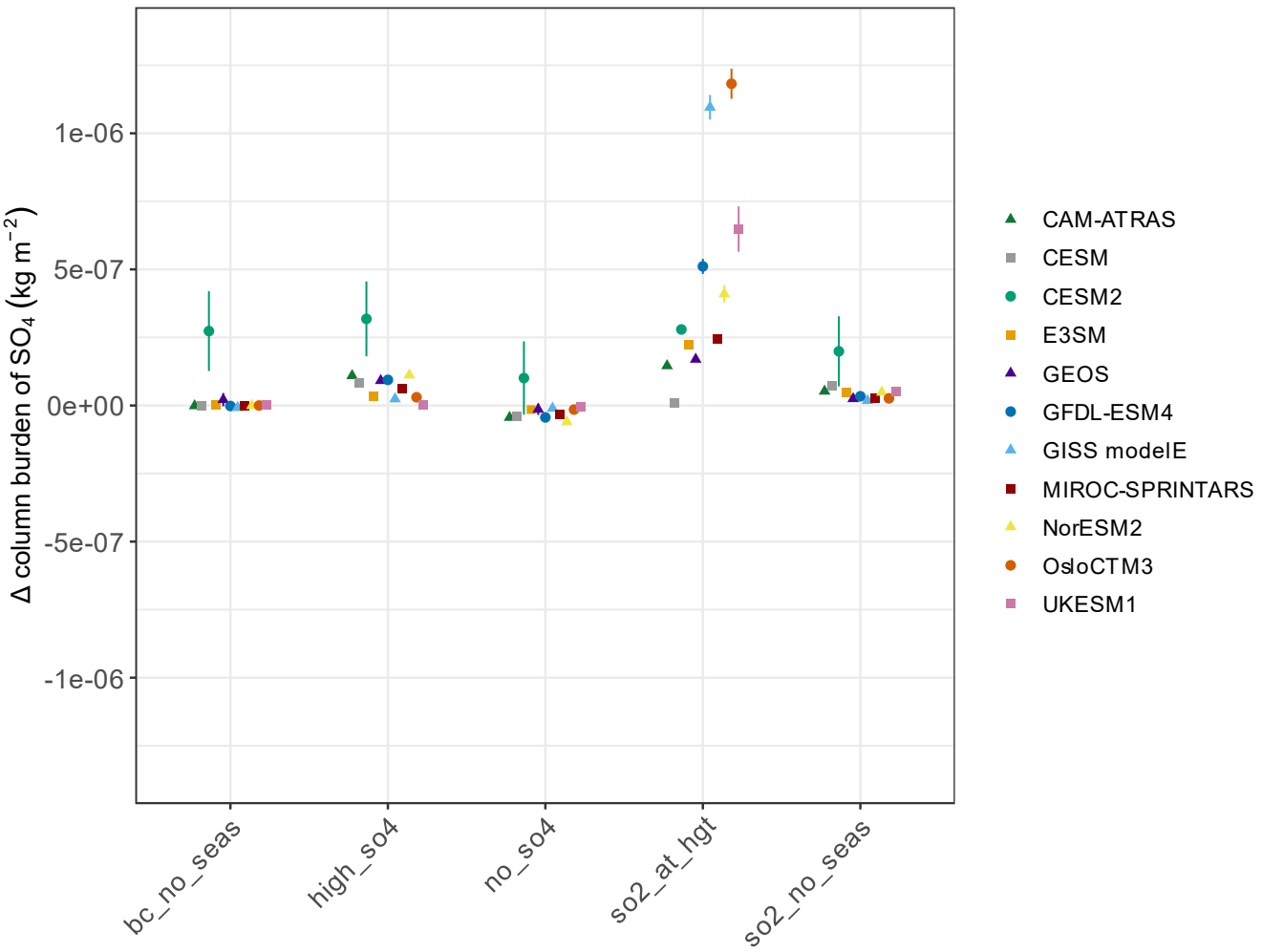


Figure S13: Absolute difference of global mean $SO_4$ column burden for each perturbation. All results are averaged over the years 2000 – 2004, except NorESM2 is averaged over 2001 – 2005. The uncertainty bars represent interannual variability (± 1 σ).

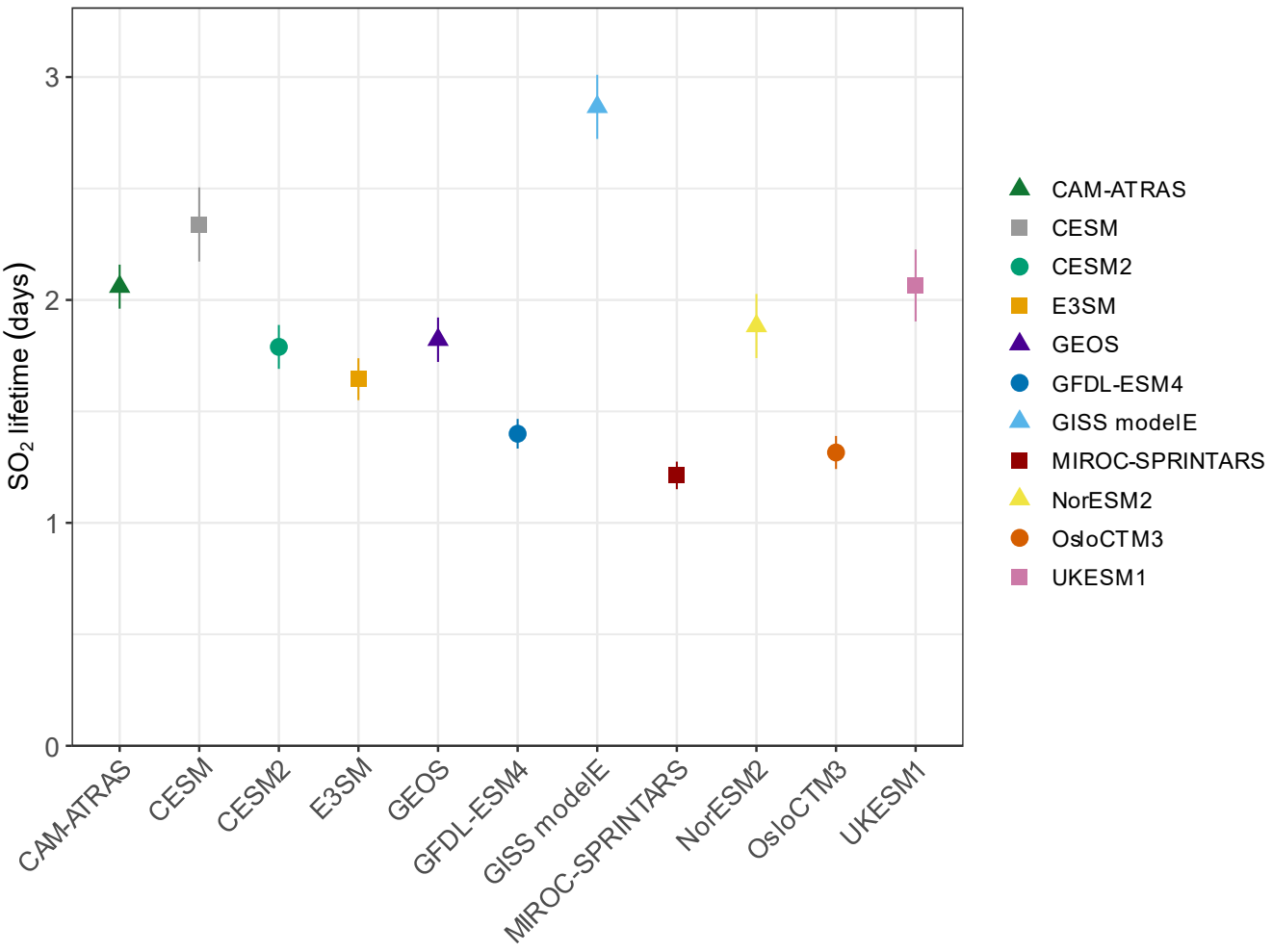


Figure S14: Northern Hemisphere land $SO_2$ lifetime of the emission at height perturbation simulations. All results are averaged over the years 2000 – 2004, except NorESM2 is averaged over 2001 – 2005. The error bars represent interannual variability (± 1 σ).

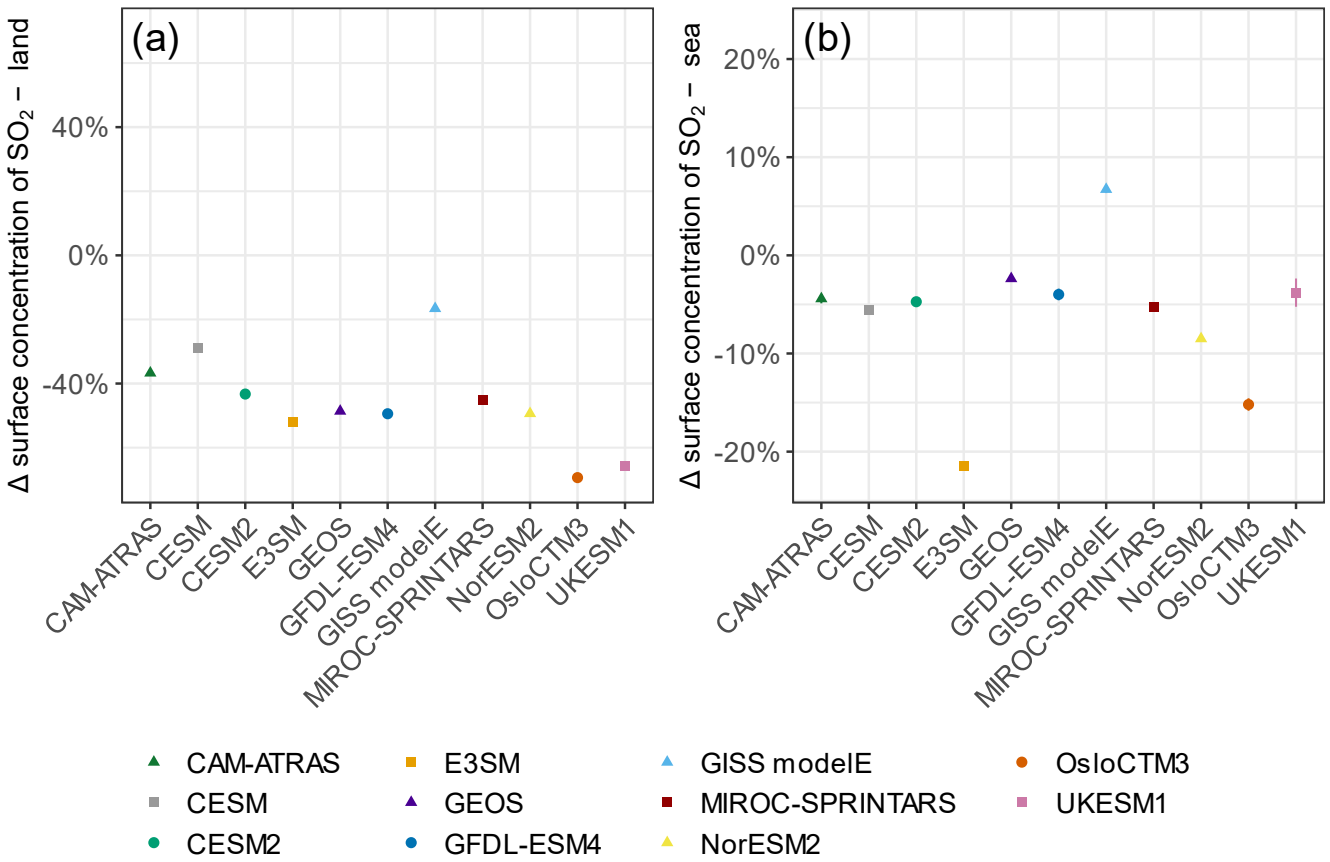


Figure S15: Percent difference (emission at height – reference) of (a) land surface concentration of $SO_2$ and (b) sea surface concentration of $SO_2$. All results are averaged over the years 2000 – 2004, except NorESM2 is averaged over 2001 – 2005. The error bars represent interannual variability (± 1 σ).

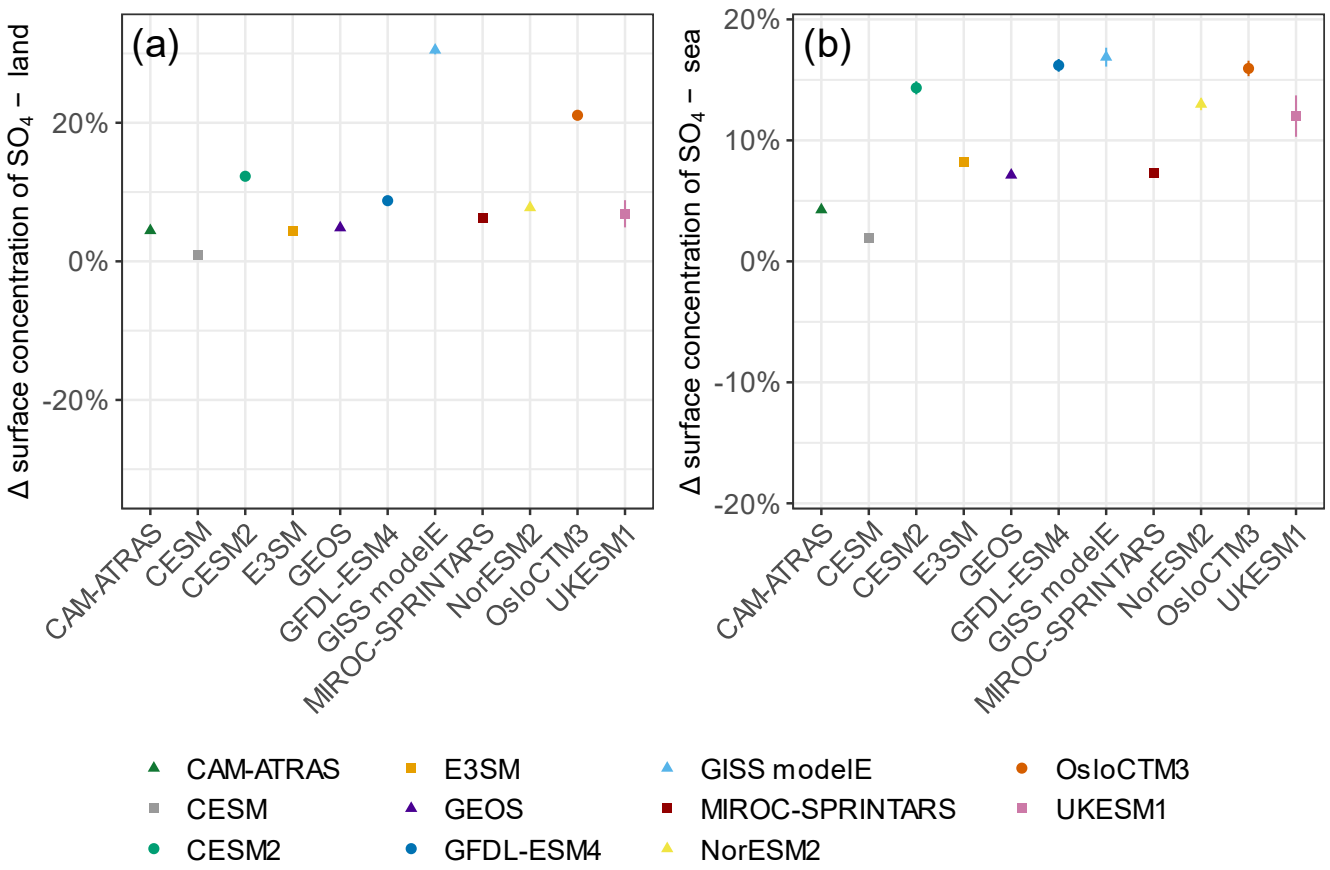


Figure S16: Percent difference (emission at height – reference) of (a) land surface concentration of $SO_4$ and (b) sea surface concentration of $SO_4$. All results are averaged over the years 2000 – 2004, except NorESM2 is averaged over 2001 – 2005. The error bars represent interannual variability (± 1 σ).

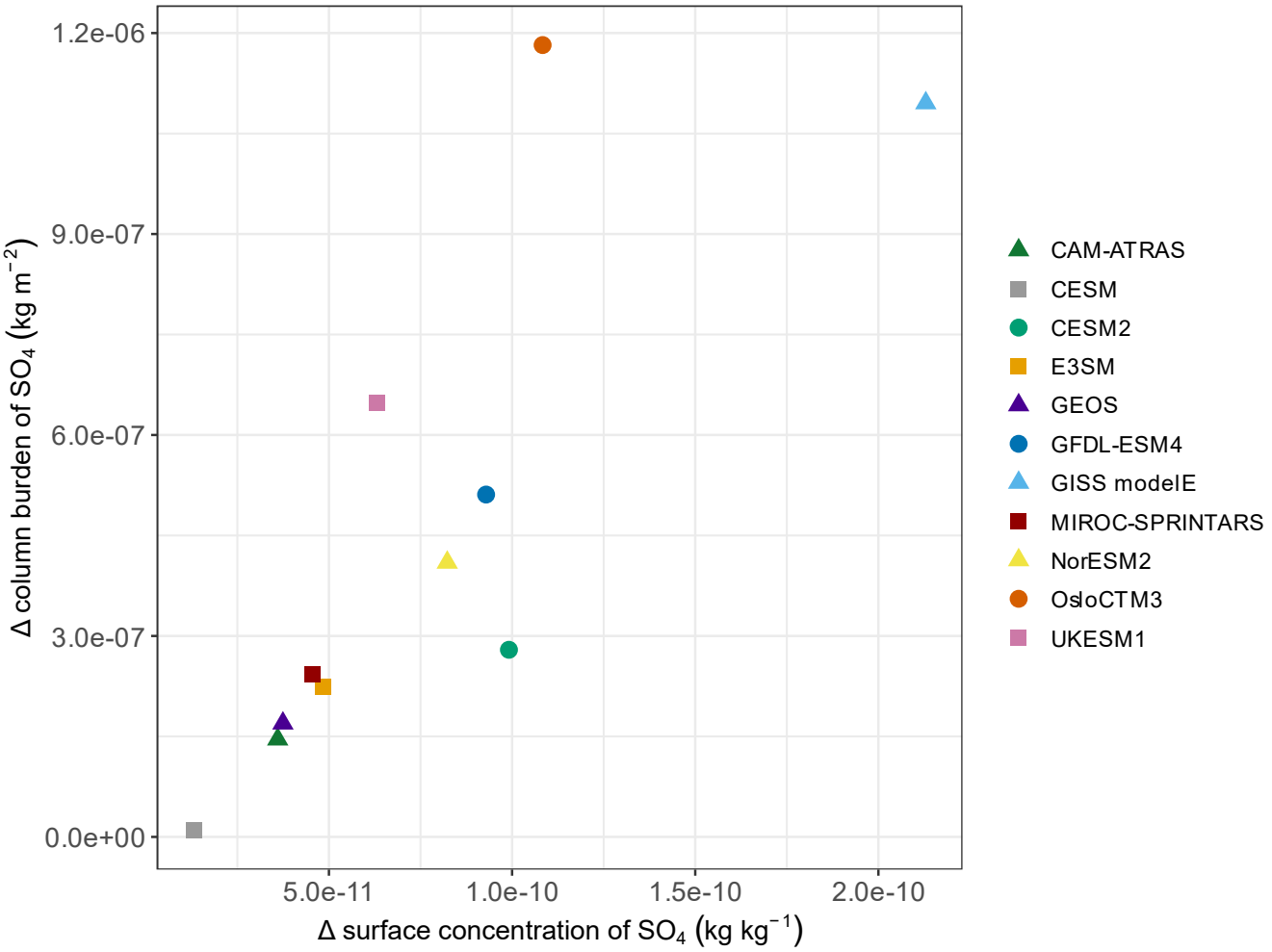


Figure S17: Absolute difference (emission at height – reference) of global mean sulfate column burden vs surface sulfate concentration. All results are averaged over the years 2000 – 2004, except NorESM2 is averaged over 2001 – 2005.

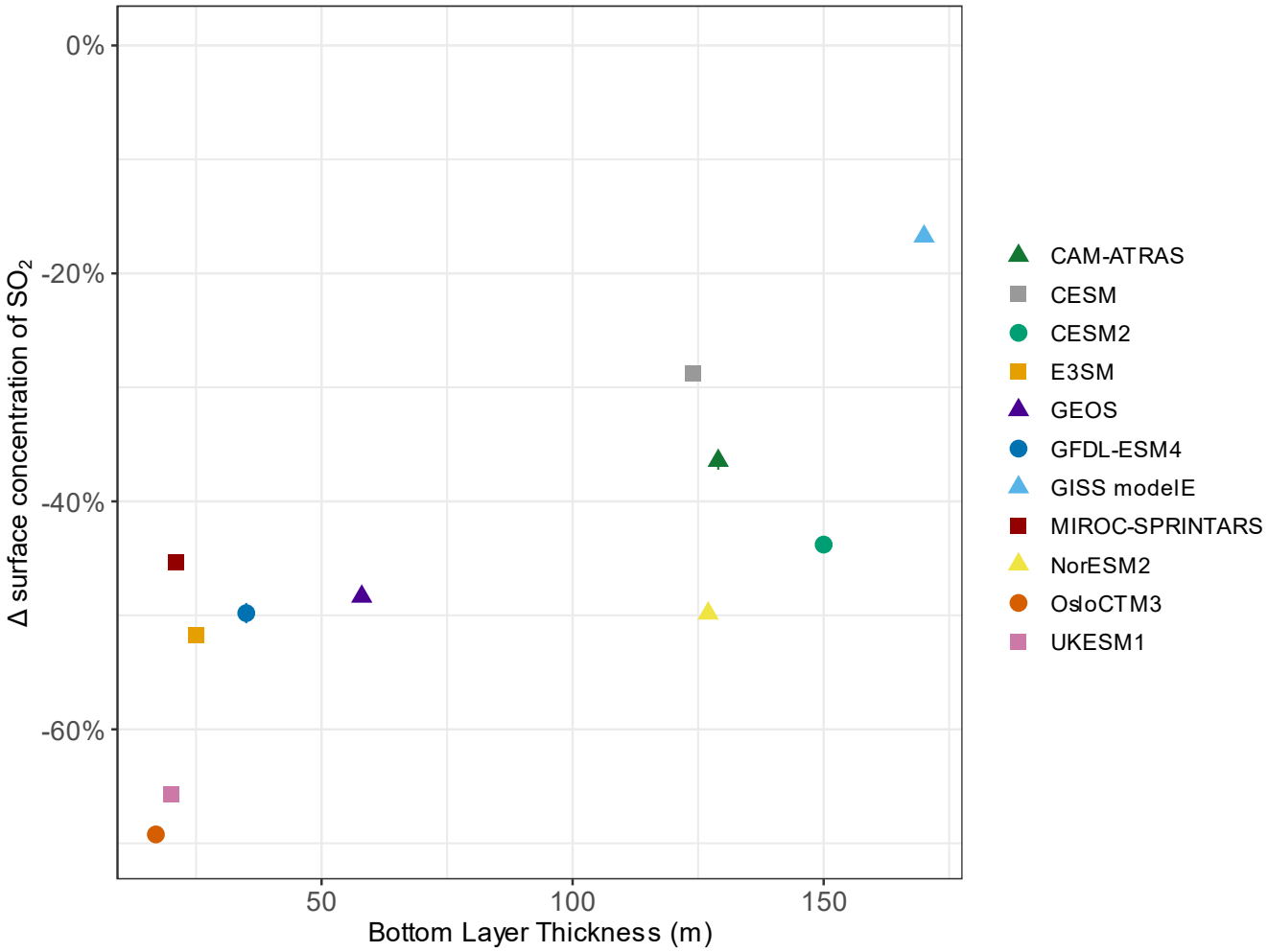


Figure S18: Percent difference (emission at height – reference) of Northern Hemisphere land $SO_2$ surface concentration vs bottom model layer thickness. All results are averaged over the years 2000 – 2004, except NorESM2 is averaged over 2001 – 2005.

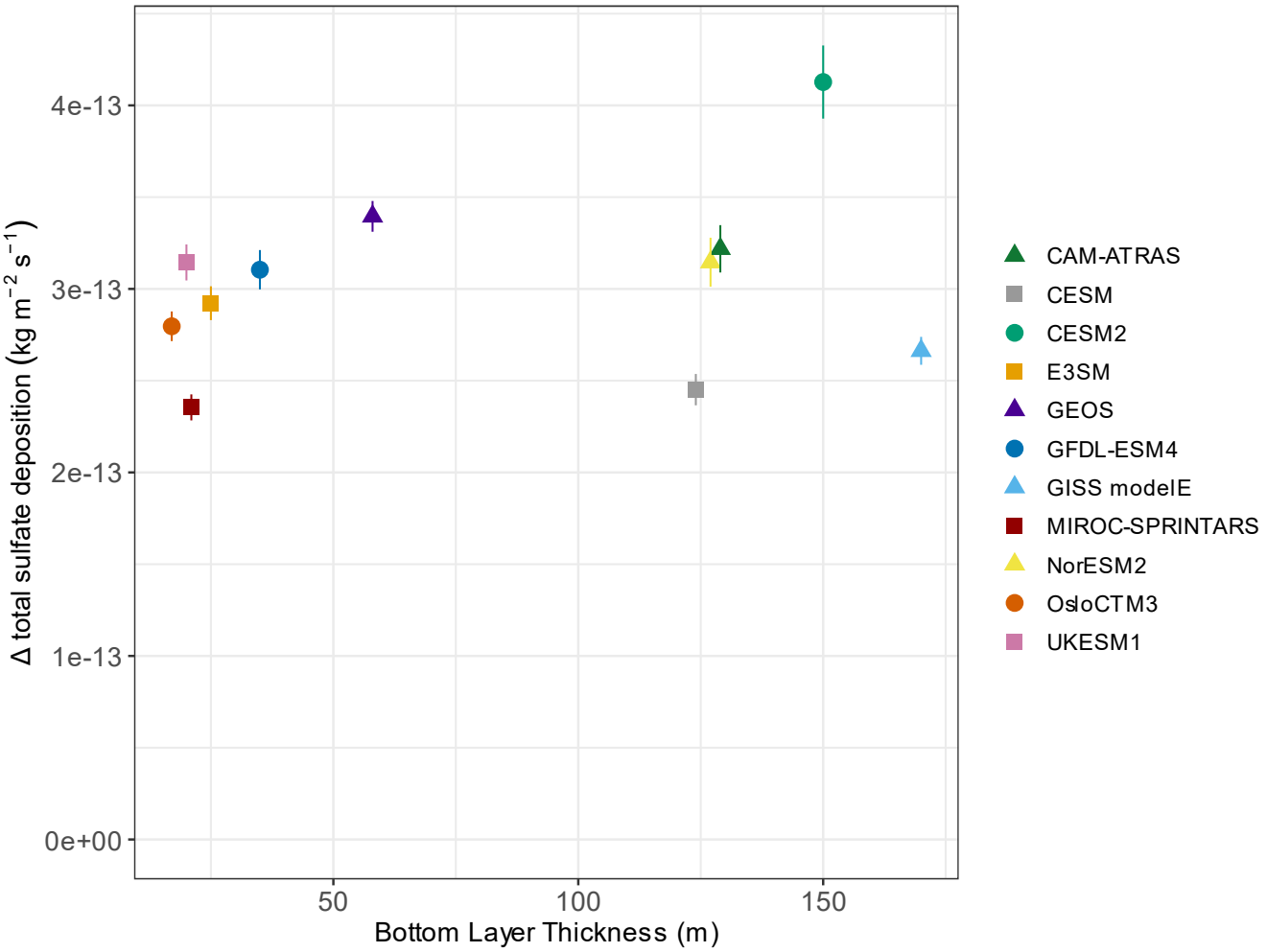


Figure S19: Absolute difference (high $SO_4$ – reference) of global mean total sulfate deposition vs bottom model layer thickness. All results are averaged over the years 2000 – 2004, except NorESM2 is averaged over 2001 – 2005. The error bars represent interannual variability (± 1 σ).

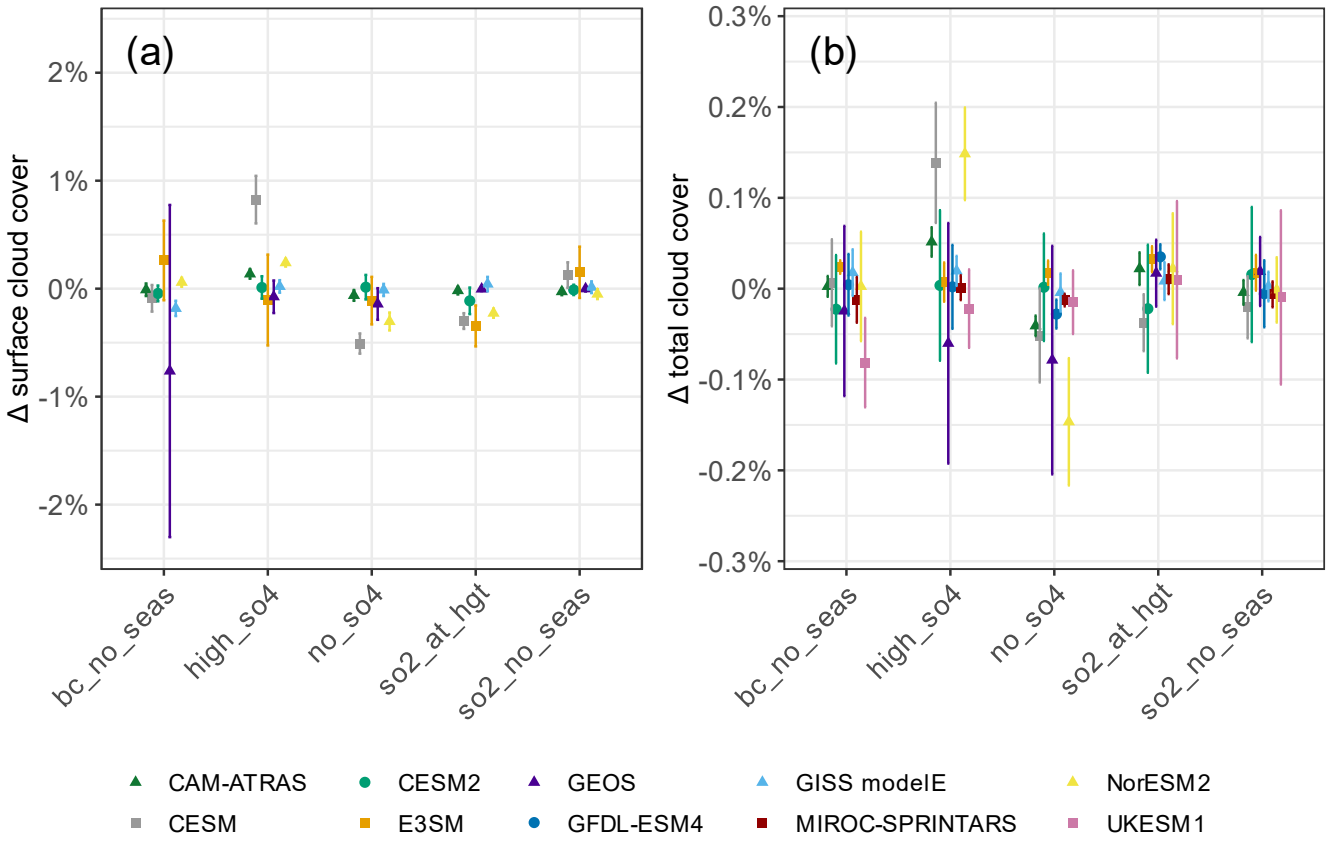


Figure S20: Percent difference of global mean (a) surface cloud cover and (b) total cloud cover for each perturbation. All results are averaged over the years 2000 – 2004, except NorESM2 is averaged over 2001 – 2005. The uncertainty bars represent interannual variability (± 1 σ).

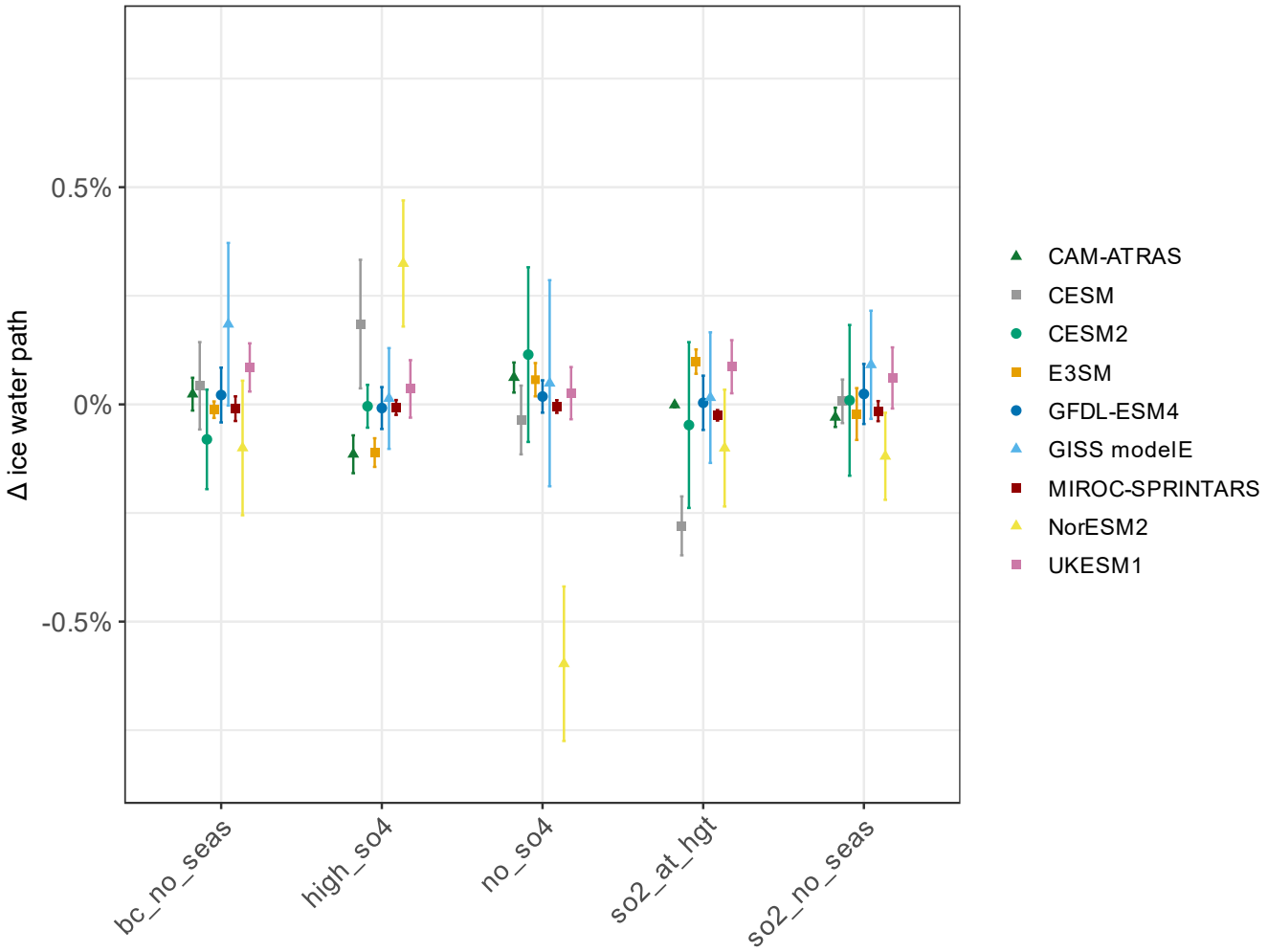


Figure S21: Percent difference of global mean ice water path for each perturbation. All results are averaged over the years 2000 – 2004, except NorESM2 is averaged over 2001 – 2005. The uncertainty bars represent interannual variability (± 1 σ).

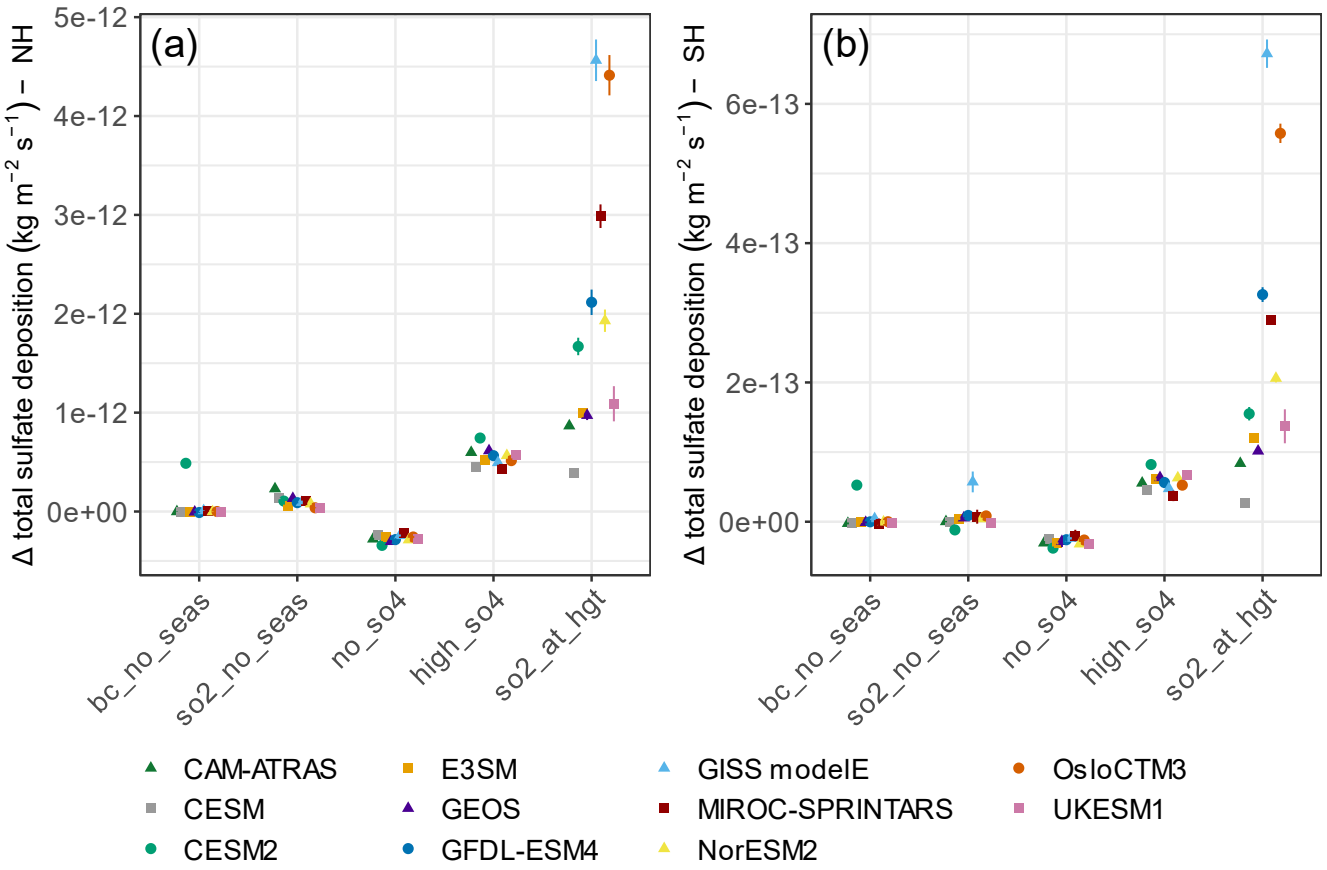


Figure S22: Absolute difference of (a) Northern Hemisphere total sulfate deposition and (b) Southern Hemisphere total sulfate deposition for each perturbation. All results are averaged over the years 2000 – 2004, except NorESM2 is averaged over 2001 – 2005. The uncertainty bars represent interannual variability (± 1 σ).

Table S1: Aerosol module characteristics[1]

| Earth System Model (component models) | Resolution | Description of aerosol module | References |
|---|---|---|---|
| E3SMv1 (EAMv1, ELMv0) | 1° × 1°, 72 vertical levels | Two-moment (mass and number) aerosol scheme with 4 lognormal modes, namely Aitken, accumulation, coarse, and primary-carbon mode.<br><br>Aerosols are internally mixed within each mode and externally mixed between modes.<br><br>Aerosol species included: sulfate, black carbon (BC), primary organic aerosol (POA); secondary | Wang et al., 2020; Liu et al., 2016 |

[1] Table format is adapted from Table S1 from the supplement of Thornhill et al., 2021 (entries for GISS-E2-1, NorESM2, GFDL-ESM4, CESM2-WACCM, MIROC6, and UKESM1 have been partially or fully copied from this table). Information for CAM-ATRAS is taken from the supplement of Fanourgakis et al., 2019.

| | | | |
|---|---|---|---|
| | | organic aerosol (SOA), marine organic aerosol (MOA), sea salt, and dust.<br><br>MAM4 explicitly treats microphysical aging of primary carbonaceous aerosols in the atmosphere by introducing the primary-carbon mode. The number of monolayers required for the aging of BC and POA particles from the primary carbon mode to the accumulation mode is set to 8. | |
| CESM1 (CAM5.3, CLM4) | 1.9° (lat) x 2.5° (lon), 30 vertical levels | Two-moment (mass and number) aerosol scheme with 4 lognormal modes, namely Aitken, accumulation, coarse, and primary-carbon mode.<br><br>Aerosols are internally mixed within each mode and externally mixed between modes.<br><br>Aerosol species included: sulfate, BC, POA, SOA, sea salt, and dust.<br><br>MAM4 explicitly treats microphysical aging of primary carbonaceous aerosols in the atmosphere by introducing the primary-carbon mode. The number of monolayers required for the aging of BC and POA particles from the primary carbon mode to the accumulation mode is set to 8. | Liu et al., 2016 |
| GISS-E2-1 (p5 variant) | 2° (lat) x 2.5° (lon), 40 vertical levels surface to 0.1 hPa | Aerosols and ozone are calculated prognostically using the MATRIX aerosol module.<br><br>Aerosol microphysics include nucleation of new particles, condensation and coagulation. The mixing state of particles is explicitly tracked. Aerosol mixtures can include, ammonium, sulfate, nitrate, organics, BC, sea salt, dust and aerosol water.<br><br>Aerosol scheme is coupled to the tropospheric chemistry scheme which includes inorganic chemistry of $O_x$, $NO_x$, $HO_x$, CO, and organic chemistry of $CH_4$ and higher hydrocarbons using the CBM4 scheme and the stratospheric chemistry scheme which includes chlorine and bromine chemistry together with polar stratospheric clouds. | Bauer et al., 2020, 2008 |
| NorESM2 | 1.9° (lat) × 2.5° (lon), 32 vertical levels | Production-tagged aerosol module with background lognormal modes (Aitken, accumulation, coarse). Process tracers can alter the shape and composition of the initially lognormal background modes to generate mixtures. | Kirkevåg et al., 2018 |

| | | | |
|---|---|---|---|
| | | OsloAero6 aerosol module which contains some slight updates since (Kirkevåg et al., 2018) describes the formation and evolution of BC, OC, $SO_4$, dust, sea-salt and SOA. There is a limited gas-phase chemistry describing the oxidation of the aerosol precursors DMS, $SO_2$, isoprene, and monoterpenes. Oxidant fields of OH, $HO_2$, $NO_3$ and $O_3$ are prescribed climatological fields. As there is no ozone chemistry in the model, prescribed monthly-varying ozone fields are used for the radiation.<br><br>Components included: sulfate, BC, organic aerosol, sea salt, dust | |
| GFDL-ESM4 | 1° × 1.25° (100 km cubed sphere), 49 vertical levels | The model includes 56 prognostic (transported) tracers and 36 diagnostic (non-transported) chemical tracers, with 43 photolysis reactions, 190 gas-phase kinetic reactions, and 15 heterogeneous reactions. The tropospheric chemistry includes reactions for the $NO_x$-$HO_x$-$O_x$-CO-$CH_4$ system and oxidation schemes for other non-methane volatile organic compounds. The stratospheric chemistry accounts for the major ozone loss cycles ($O_x$, $HO_x$, $NO_x$, $ClO_x$, and $BrO_x$) and heterogeneous reactions on liquid and solid stratospheric aerosols as in Austin et al. (2013). The bulk aerosol scheme, including 18 transported aerosol tracers, is similar to that in AM4.0 (Zhao et al., 2018), with the following updates: (1) ammonium and nitrate aerosols are treated explicitly, with ISORROPIA (Fountoukis and Nenes, 2007) used to simulate the sulfate–nitrate–ammonia thermodynamic equilibrium; (2) oxidation of sulfur dioxide and dimethyl sulfide to produce sulfate aerosol is driven by the gas-phase oxidant concentrations (OH, $H_2O_2$, and $O_3$) and cloud pH simulated by the online chemistry scheme, and (3) the rate of aging of black and organic carbon aerosols from hydrophobic to hydrophilic forms varies with calculated concentrations of hydroxyl radical (OH). Aerosol species, including sulfate, BC, organic aerosols, sea-salt, dust and nitrate are treated explicitly. | Horowitz et al., 2020; Dunne et al., 2020 |
| CESM2-WACCM | 0.9° (lat) × 1.25° (lon), 88 vertical levels | Chemistry and aerosols for the troposphere, stratosphere, mesosphere and lower thermosphere are calculated interactively. It simulates 228 compounds, including the 4-mode Modal Aerosol Model (MAM4). This version of MAM4 is modified | Emmons et al., 2020; Danabasoglu et al., 2020; Gettelman et al., 2019; Tilmes et al., 2019; Mills et al., 2016 |

| | | | |
|---|---|---|---|
| | | to allow for the simulation of stratospheric aerosols from volcanic eruptions (from their $SO_2$ emissions) and oxidation of OCS. The representation of secondary organic aerosols follows the Volatility Basis Set approach. | |
| OsloCTM3 | 2.25° (lat) × 2.25° (lon), 60 vertical levels | The BC scheme in OsloCTM3 is a bulk-scheme, with transfer from hydrophobic to hydrophilic mode represented by an aging rate that depends on month and latitude. Upon emission 20% of BC is assumed to be hydrophilic and 80% hydrophobic. The BC aerosol from biofuel, fossil fuel and biomass burning are treated separately. For BC from fossil fuel and biofuel, a mass absorption coefficient parametrization is used based on observations from Zanatta et al. (2016) and depends on coating from non-BC, see further details in Lund et al. (2018). The sulfur scheme with dimethyl sulfide (DMS), $SO_2$, sulfate, $H_2S$, and methanesulfonic acid (MSA) is described in Berglen et al. (2004). The scheme is interactively linked to the tropospheric chemistry in OsloCTM3 and includes gas-phase and aqueous-phase oxidation of $SO_2$. Optical properties for sulfate are described in Myhre et al. (2007). | Lund et al., 2018; Zanatta et al., 2016; Myhre et al., 2007; Berglen, 2004 |
| GEOS | 0.5° (lat) x 0.625° (lon), 72 vertical levels | Bulk mass aerosol scheme named GOCART.<br><br>Components included: sulfate, BC, organic aerosol, sea salt, dust, $NO_3$, $NH_4$<br><br>BC, organic aerosol, sulfate, and $NH_4$ are in accumulation mode. $NO_3$, sea salt, and dust covers accumulation and coarse modes with 3 bins, 5 bins, and 5 bins, respectively.<br><br>DMS emissions are calculated based on DMS seawater concentration compiled by Lana et al., (2011) combining with online meteorological fields.<br><br>Oxidant fields (e.g., OH, $H_2O_2$ and $O_3$) are prescribed from previous GEOS chemistry climate model (GEOSCCM) simulations (Strode et al., 2019). | Strode et al., 2018; Bian et al., 2017; Colarco et al., 2010; Chin et al., 2000 |
| MIROC6 | 0.5625˚ × ~0.5625˚ | Spectral Radiation-Transport Model for Aerosol Species (SPRINTARS) predicts mass mixing ratios of the main tropospheric aerosols, and models aerosol-cloud interactions in which aerosols alter cloud microphysical properties and affect the radiation budget by acting as cloud condensation and ice nuclei. The $SO_4$, BC and OC aerosols are treated as externally mixed in this model. The | Takemura et al., 2009; Takemura, 2005 |

| | | | |
|---|---|---|---|
| | | CDNC and ice crystal number are used to calculate the aerosol indirect effect and cloud nucleation process.<br><br>Components included: sulfate, BC, OA, sea salt, dust | |
| UKESM1 | 1.25° (lat) x 1.875° (lon), 85 vertical levels | The model contains the GLOMAP-mode aerosol microphysics scheme.<br><br>Two-moment (mass and number) aerosol scheme with 5 lognormal modes (nucleation soluble, Aitken soluble, Aitken insoluble, accumulation soluble, coarse soluble).<br><br>Components included: sulfate, BC, OA, sea salt, dust*<br><br>*Dust component tracked independently in six size bins<br><br>An adapted version of UKESM1 with non-interactive chemistry was used. Oxidant fields (OH and $O_3$) were prescribed using monthly mean output from the full-chemistry (and fully coupled, i.e. interactive land surface, ocean and ocean biogeochemistry) version of UKESM averaged over 1979 to 2014.<br><br>The aerosol scheme, called GLOMAP-mode, is a two-moment scheme for the simulation of tropospheric BC, OC, $SO_4$, and sea salt. Dust is modelled independently using the bin scheme of Woodward (2001). The chemistry and aerosol schemes are coupled such that the secondary aerosol ($SO_4$, OA) formation rates depend on oxidants from the stratosphere-troposphere chemistry scheme. Aerosol particles are activated into cloud droplets using the activation scheme of Abdul-Razzak and Ghan (2000) which is dependent on aerosol size distribution, aerosol composition, and meteorological conditions. Changes in CDNC affect cloud droplet effective radius ((Jones et al., 2001) and the auto conversion of cloud liquid water in to rain water (Khairoutdinov and Kogan, 2000), which both influence cloud albedo. Stratospheric aerosols (aerosol optical depth and surface area density) are prescribed in the model (Sellar et al., 2019b). | Regayre et al., 2022; Mulcahy et al., 2020; Sellar et al., 2019; Williams et al., 2018 |

| | | | |
|---|---|---|---|
| CAM-ATRAS | 1.9° (lat) × 2.5° (lon), 30 vertical levels | The CAM5-chem-ATRAS2 uses the Aerosol Two-dimensional bin module for foRmation and Aging Simulation version 2 (ATRAS2) (Matsui, 2017; Matsui and Mahowald, 2017). The ATRAS2 model uses 12 size bins from 0.001 to 10 μm in aerosol dry diameter. BC mixing state is resolved with 8, 3, or 1 bins for each size bin. Mass concentrations of eight aerosol species ($SO_4$, $NO_3$, $NH_4$, dust, sea salt, OA (POA+SOA), BC, and water) and number concentrations are calculated for each bin in the model. The CAM5-chem-ATRAS2 model considers emissions, gas-phase chemistry, condensation and evaporation of $SO_4$, $NO_3$, $NH_4$, and OA, coagulation, nucleation, activation of aerosol and evaporation from cloud, aerosol formation in clouds, dry and wet deposition, aerosol optical properties, aerosol-radiation interactions, and aerosol-cloud interactions. OA formation is calculated by a volatility basis-set approach which considers oxidations of POA (gas-phase), alkanes, alkenes, aromatics, isoprene, and monoterpene (Matsui et al., 2014; Matsui, 2017). Nucleation is calculated by the activation-type theory (Kulmala et al., 2006) within the planetary boundary layer and by a binary homogeneous nucleation scheme (Vehkamäki et al., 2002) within the free troposphere. | Sand et al., 2021; Gliß et al., 2021; Burgos et al., 2020; Fanourgakis et al., 2019 |

Table S2: Tabulated values of Figure S9 showing relative impact of deposition vs chemical conversion when estimating change in $SO_2$ lifetime over Northern Hemisphere land due to emission at height.

| model | $\Delta SO_2$ lifetime | $\Delta SO_2$ lifetime (change in deposition rate only) | ratio |
|---|---|---|---|
| CAM-ATRAS | 0.15 | 0.28 | 1.84 |
| CESM | 0.14 | | |
| CESM2 | 0.30 | 0.53 | 1.74 |
| E3SM | 0.26 | 0.34 | 1.30 |
| GEOS | 0.32 | 0.49 | 1.50 |
| GFDL-ESM4 | 0.44 | 0.67 | 1.51 |
| GISS modelE | 0.80 | 1.55 | 1.94 |
| MIROC-SPRINTARS | 0.25 | 0.46 | 1.84 |
| NorESM2 | 0.26 | 0.47 | 1.79 |
| OsloCTM3 | 0.45 | 0.89 | 1.96 |
| UKESM1 | 0.47 | 0.81 | 1.74 |
| Avg | 0.35 | 0.65 | 1.72 |
| Avg (w/o GISS modelE) | 0.31 | 0.55 | 1.69 |

**References**


Bauer, S. E., Wright, D. L., Koch, D., Lewis, E. R., McGraw, R., Chang, L.-S., Schwartz, S. E., and Ruedy, R.: MATRIX (Multiconfiguration Aerosol TRacker of mIXing state): an aerosol microphysical module for global atmospheric models, Atmospheric Chem. Phys., 8, 6003–6035, https://doi.org/10.5194/acp-8-6003-2008, 2008.

Bauer, S. E., Tsigaridis, K., Faluvegi, G., Kelley, M., Lo, K. K., Miller, R. L., Nazarenko, L., Schmidt, G. A., and Wu, J.: Historical (1850–2014) Aerosol Evolution and Role on Climate Forcing Using the GISS ModelE2.1 Contribution to CMIP6, J. Adv. Model. Earth Syst., 12, https://doi.org/10.1029/2019MS001978, 2020.

Berglen, T. F.: A global model of the coupled sulfur/oxidant chemistry in the troposphere: The sulfur cycle, J. Geophys. Res., 109, D19310, https://doi.org/10.1029/2003JD003948, 2004.

Bian, H., Chin, M., Hauglustaine, D. A., Schulz, M., Myhre, G., Bauer, S. E., Lund, M. T., Karydis, V. A., Kucsera, T. L., Pan, X., Pozzer, A., Skeie, R. B., Steenrod, S. D., Sudo, K., Tsigaridis, K., Tsimpidi, A. P., and Tsyro, S. G.: Investigation of global particulate nitrate from the AeroCom phase III experiment, Atmospheric Chem. Phys., 17, 12911–12940, https://doi.org/10.5194/acp-17-12911-2017, 2017.

Burgos, M. A., Andrews, E., Titos, G., Benedetti, A., Bian, H., Buchard, V., Curci, G., Kipling, Z., Kirkevåg, A., Kokkola, H., Laakso, A., Letertre-Danczak, J., Lund, M. T., Matsui, H., Myhre, G., Randles, C., Schulz, M., Van Noije, T., Zhang, K., Alados-Arboledas, L., Baltensperger, U., Jefferson, A., Sherman, J., Sun, J., Weingartner, E., and Zieger, P.: A global model–measurement evaluation of particle light scattering coefficients at elevated relative humidity, Atmospheric Chem. Phys., 20, 10231–10258, https://doi.org/10.5194/acp-20-10231-2020, 2020.

Chin, M., Savoie, D. L., Huebert, B. J., Bandy, A. R., Thornton, D. C., Bates, T. S., Quinn, P. K., Saltzman, E. S., and De Bruyn, W. J.: Atmospheric sulfur cycle simulated in the global model GOCART: Comparison with field observations and regional budgets, J. Geophys. Res. Atmospheres, 105, 24689–24712, https://doi.org/10.1029/2000JD900385, 2000.

Colarco, P., da Silva, A., Chin, M., and Diehl, T.: Online simulations of global aerosol distributions in the NASA GEOS-4 model and comparisons to satellite and ground-based aerosol optical depth, J. Geophys. Res., 115, D14207, https://doi.org/10.1029/2009JD012820, 2010.

Danabasoglu, G., Lamarque, J. -F., Bacmeister, J., Bailey, D. A., DuVivier, A. K., Edwards, J., Emmons, L. K., Fasullo, J., Garcia, R., Gettelman, A., Hannay, C., Holland, M. M., Large, W. G., Lauritzen, P. H., Lawrence, D. M., Lenaerts, J. T. M., Lindsay, K., Lipscomb, W. H., Mills, M. J., Neale, R., Oleson, K. W., Otto-Bliesner, B., Phillips, A. S., Sacks, W., Tilmes, S., Van Kampenhout, L., Vertenstein, M., Bertini, A., Dennis, J., Deser, C., Fischer, C., Fox-Kemper, B., Kay, J. E., Kinnison, D., Kushner, P. J., Larson, V. E., Long, M. C., Mickelson, S., Moore, J. K., Nienhouse, E., Polvani, L., Rasch, P. J., and Strand, W. G.: The Community Earth System Model Version 2 (CESM2), J. Adv. Model. Earth Syst., 12, e2019MS001916, https://doi.org/10.1029/2019MS001916, 2020.

Dunne, J. P., Horowitz, L. W., Adcroft, A. J., Ginoux, P., Held, I. M., John, J. G., Krasting, J. P., Malyshev, S., Naik, V., Paulot, F., Shevliakova, E., Stock, C. A., Zadeh, N., Balaji, V., Blanton, C., Dunne, K. A., Dupuis, C., Durachta, J., Dussin, R., Gauthier, P. P. G., Griffies, S. M., Guo, H., Hallberg, R. W., Harrison, M., He, J., Hurlin, W., McHugh, C., Menzel, R., Milly, P. C. D., Nikonov, S., Paynter, D. J., Ploshay, J., Radhakrishnan, A., Rand, K., Reichl, B. G., Robinson, T., Schwarzkopf, D. M., Sentman, L. T., Underwood, S., Vahlenkamp, H., Winton, M., Wittenberg, A. T., Wyman, B., Zeng, Y., and Zhao, M.: The GFDL Earth System Model Version 4.1 (GFDL-ESM 4.1): Overall Coupled Model Description and Simulation Characteristics, J. Adv. Model. Earth Syst., 12, e2019MS002015, https://doi.org/10.1029/2019MS002015, 2020.

Emmons, L. K., Schwantes, R. H., Orlando, J. J., Tyndall, G., Kinnison, D., Lamarque, J., Marsh, D., Mills, M. J., Tilmes, S., Bardeen, C., Buchholz, R. R., Conley, A., Gettelman, A., Garcia, R., Simpson, I., Blake, D. R., Meinardi, S., and Pétron, G.: The Chemistry Mechanism in the Community Earth System Model Version 2 (CESM2), J. Adv. Model. Earth Syst., 12, https://doi.org/10.1029/2019MS001882, 2020.

Fanourgakis, G. S., Kanakidou, M., Nenes, A., Bauer, S. E., Bergman, T., Carslaw, K. S., Grini, A., Hamilton, D. S., Johnson, J. S., Karydis, V. A., Kirkevåg, A., Kodros, J. K., Lohmann, U., Luo, G., Makkonen, R., Matsui, H., Neubauer, D.,

Pierce, J. R., Schmale, J., Stier, P., Tsigaridis, K., Van Noije, T., Wang, H., Watson-Parris, D., Westervelt, D. M., Yang, Y., Yoshioka, M., Daskalakis, N., Decesari, S., Gysel-Beer, M., Kalivitis, N., Liu, X., Mahowald, N. M., Myriokefalitakis, S., Schrödner, R., Sfakianaki, M., Tsimpidi, A. P., Wu, M., and Yu, F.: Evaluation of global simulations of aerosol particle and cloud condensation nuclei number, with implications for cloud droplet formation, Atmospheric Chem. Phys., 19, 8591–8617, https://doi.org/10.5194/acp-19-8591-2019, 2019.

Gettelman, A., Hannay, C., Bacmeister, J. T., Neale, R. B., Pendergrass, A. G., Danabasoglu, G., Lamarque, J. -F., Fasullo, J. T., Bailey, D. A., Lawrence, D. M., and Mills, M. J.: High Climate Sensitivity in the Community Earth System Model Version 2 (CESM2), Geophys. Res. Lett., 46, 8329–8337, https://doi.org/10.1029/2019GL083978, 2019.

Gliß, J., Mortier, A., Schulz, M., Andrews, E., Balkanski, Y., Bauer, S. E., Benedictow, A. M. K., Bian, H., Checa-Garcia, R., Chin, M., Ginoux, P., Griesfeller, J. J., Heckel, A., Kipling, Z., Kirkevåg, A., Kokkola, H., Laj, P., Le Sager, P., Lund, M. T., Lund Myhre, C., Matsui, H., Myhre, G., Neubauer, D., van Noije, T., North, P., Olivié, D. J. L., Rémy, S., Sogacheva, L., Takemura, T., Tsigaridis, K., and Tsyro, S. G.: AeroCom phase III multi-model evaluation of the aerosol life cycle and optical properties using ground- and space-based remote sensing as well as surface in situ observations, Atmospheric Chem. Phys., 21, 87–128, https://doi.org/10.5194/acp-21-87-2021, 2021.

Horowitz, L. W., Naik, V., Paulot, F., Ginoux, P. A., Dunne, J. P., Mao, J., Schnell, J., Chen, X., He, J., John, J. G., Lin, M., Lin, P., Malyshev, S., Paynter, D., Shevliakova, E., and Zhao, M.: The GFDL Global Atmospheric Chemistry-Climate Model AM4.1: Model Description and Simulation Characteristics, J. Adv. Model. Earth Syst., 12, https://doi.org/10.1029/2019MS002032, 2020.

Kirkevåg, A., Grini, A., Olivié, D., Seland, Ø., Alterskjær, K., Hummel, M., Karset, I. H. H., Lewinschal, A., Liu, X., Makkonen, R., Bethke, I., Griesfeller, J., Schulz, M., and Iversen, T.: A production-tagged aerosol module for Earth system models, OsloAero5.3 – extensions and updates for CAM5.3-Oslo, Geosci. Model Dev., 11, 3945–3982, https://doi.org/10.5194/gmd-11-3945-2018, 2018.

Liu, X., Ma, P.-L., Wang, H., Tilmes, S., Singh, B., Easter, R. C., Ghan, S. J., and Rasch, P. J.: Description and evaluation of a new four-mode version of the Modal Aerosol Module (MAM4) within version 5.3 of the Community Atmosphere Model, Geosci. Model Dev., 9, 505–522, https://doi.org/10.5194/gmd-9-505-2016, 2016.

Lund, M. T., Myhre, G., Haslerud, A. S., Skeie, R. B., Griesfeller, J., Platt, S. M., Kumar, R., Myhre, C. L., and Schulz, M.: Concentrations and radiative forcing of anthropogenic aerosols from 1750 to 2014 simulated with the Oslo CTM3 and CEDS emission inventory, Geosci. Model Dev., 11, 4909–4931, https://doi.org/10.5194/gmd-11-4909-2018, 2018.

Mills, M. J., Schmidt, A., Easter, R., Solomon, S., Kinnison, D. E., Ghan, S. J., Neely, R. R., Marsh, D. R., Conley, A., Bardeen, C. G., and Gettelman, A.: Global volcanic aerosol properties derived from emissions, 1990–2014, using CESM1(WACCM), J. Geophys. Res. Atmospheres, 121, 2332–2348, https://doi.org/10.1002/2015JD024290, 2016.

Mulcahy, J. P., Johnson, C., Jones, C. G., Povey, A. C., Scott, C. E., Sellar, A., Turnock, S. T., Woodhouse, M. T., Abraham, N. L., Andrews, M. B., Bellouin, N., Browse, J., Carslaw, K. S., Dalvi, M., Folberth, G. A., Glover, M., Grosvenor, D. P., Hardacre, C., Hill, R., Johnson, B., Jones, A., Kipling, Z., Mann, G., Mollard, J., O'Connor, F. M., Palmiéri, J., Reddington, C., Rumbold, S. T., Richardson, M., Schutgens, N. A. J., Stier, P., Stringer, M., Tang, Y., Walton, J., Woodward, S., and Yool, A.: Description and evaluation of aerosol in UKESM1 and HadGEM3-GC3.1 CMIP6 historical simulations, Geosci. Model Dev., 13, 6383–6423, https://doi.org/10.5194/gmd-13-6383-2020, 2020.

Myhre, G., Bellouin, N., Berglen, T. F., Berntsen, T. K., Boucher, O., Grini, A., Isaksen, I. S. A., Johnsrud, M., Mishchenko, M. I., Stordal, F., and Tanré, D.: Comparison of the radiative properties and direct radiative effect of aerosols from a global aerosol model and remote sensing data over ocean, Tellus B, 59, 115–129, https://doi.org/10.1111/j.1600-0889.2006.00226.x, 2007.

Regayre, L. A., Deaconu, L., Grosvenor, D. P., Sexton, D., Symonds, C. C., Langton, T., Watson-Paris, D., Mulcahy, J. P., Pringle, K. J., Richardson, M., Johnson, J. S., Rostron, J., Gordon, H., Lister, G., Stier, P., and Carslaw, K. S.: Identifying climate model structural inconsistencies allows for tight constraint of aerosol radiative forcing, https://doi.org/10.5194/egusphere-2022-1330, 2022.

Sand, M., Samset, B. H., Myhre, G., Gliß, J., Bauer, S. E., Bian, H., Chin, M., Checa-Garcia, R., Ginoux, P., Kipling, Z., Kirkevåg, A., Kokkola, H., Le Sager, P., Lund, M. T., Matsui, H., Van Noije, T., Olivié, D. J. L., Remy, S., Schulz, M., Stier, P., Stjern, C. W., Takemura, T., Tsigaridis, K., Tsyro, S. G., and Watson-Parris, D.: Aerosol absorption in global models from AeroCom phase III, Atmospheric Chem. Phys., 21, 15929–15947, https://doi.org/10.5194/acp-21-15929-2021, 2021.

Sellar, A. A., Jones, C. G., Mulcahy, J. P., Tang, Y., Yool, A., Wiltshire, A., O'Connor, F. M., Stringer, M., Hill, R., Palmieri, J., Woodward, S., Mora, L., Kuhlbrodt, T., Rumbold, S. T., Kelley, D. I., Ellis, R., Johnson, C. E., Walton, J., Abraham, N. L., Andrews, M. B., Andrews, T., Archibald, A. T., Berthou, S., Burke, E., Blockley, E., Carslaw, K., Dalvi, M., Edwards, J., Folberth, G. A., Gedney, N., Griffiths, P. T., Harper, A. B., Hendry, M. A., Hewitt, A. J., Johnson, B., Jones, A., Jones, C. D., Keeble, J., Liddicoat, S., Morgenstern, O., Parker, R. J., Predoi, V., Robertson, E., Siahaan, A., Smith, R. S., Swaminathan, R., Woodhouse, M. T., Zeng, G., and Zerroukat, M.: UKESM1: Description and Evaluation of the U.K. Earth System Model, J. Adv. Model. Earth Syst., 11, 4513–4558, https://doi.org/10.1029/2019MS001739, 2019.

Strode, S. A., Liu, J., Lait, L., Commane, R., Daube, B., Wofsy, S., Conaty, A., Newman, P., and Prather, M.: Forecasting carbon monoxide on a global scale for the ATom-1 aircraft mission: insights from airborne and satellite observations and modeling, Atmospheric Chem. Phys., 18, 10955–10971, https://doi.org/10.5194/acp-18-10955-2018, 2018.

Takemura, T.: Simulation of climate response to aerosol direct and indirect effects with aerosol transport-radiation model, J. Geophys. Res., 110, D02202, https://doi.org/10.1029/2004JD005029, 2005.

Takemura, T., Egashira, M., Matsuzawa, K., Ichijo, H., O'ishi, R., and Abe-Ouchi, A.: A simulation of the global distribution and radiative forcing of soil dust aerosols at the Last Glacial Maximum, Atmospheric Chem. Phys., 9, 3061–3073, https://doi.org/10.5194/acp-9-3061-2009, 2009.

Thornhill, G. D., Collins, W. J., Kramer, R. J., Olivié, D., Skeie, R. B., O'Connor, F. M., Abraham, N. L., Checa-Garcia, R., Bauer, S. E., Deushi, M., Emmons, L. K., Forster, P. M., Horowitz, L. W., Johnson, B., Keeble, J., Lamarque, J.-F., Michou, M., Mills, M. J., Mulcahy, J. P., Myhre, G., Nabat, P., Naik, V., Oshima, N., Schulz, M., Smith, C. J., Takemura, T., Tilmes, S., Wu, T., Zeng, G., and Zhang, J.: Effective radiative forcing from emissions of reactive gases and aerosols – a multi-model comparison, Atmospheric Chem. Phys., 21, 853–874, https://doi.org/10.5194/acp-21-853-2021, 2021.

Tilmes, S., Hodzic, A., Emmons, L. K., Mills, M. J., Gettelman, A., Kinnison, D. E., Park, M., Lamarque, J. -F., Vitt, F., Shrivastava, M., Campuzano-Jost, P., Jimenez, J. L., and Liu, X.: Climate Forcing and Trends of Organic Aerosols in the Community Earth System Model (CESM2), J. Adv. Model. Earth Syst., 11, 4323–4351, https://doi.org/10.1029/2019MS001827, 2019.

Wang, H., Easter, R. C., Zhang, R., Ma, P., Singh, B., Zhang, K., Ganguly, D., Rasch, P. J., Burrows, S. M., Ghan, S. J., Lou, S., Qian, Y., Yang, Y., Feng, Y., Flanner, M., Leung, L. R., Liu, X., Shrivastava, M., Sun, J., Tang, Q., Xie, S., and Yoon, J.: Aerosols in the E3SM Version 1: New Developments and Their Impacts on Radiative Forcing, J. Adv. Model. Earth Syst., 12, https://doi.org/10.1029/2019MS001851, 2020.

Williams, K. D., Copsey, D., Blockley, E. W., Bodas-Salcedo, A., Calvert, D., Comer, R., Davis, P., Graham, T., Hewitt, H. T., Hill, R., Hyder, P., Ineson, S., Johns, T. C., Keen, A. B., Lee, R. W., Megann, A., Milton, S. F., Rae, J. G. L., Roberts, M. J., Scaife, A. A., Schiemann, R., Storkey, D., Thorpe, L., Watterson, I. G., Walters, D. N., West, A., Wood, R. A., Woollings, T., and Xavier, P. K.: The Met Office Global Coupled Model 3.0 and 3.1 (GC3.0 and GC3.1) Configurations, J. Adv. Model. Earth Syst., 10, 357–380, https://doi.org/10.1002/2017MS001115, 2018.

Zanatta, M., Gysel, M., Bukowiecki, N., Müller, T., Weingartner, E., Areskoug, H., Fiebig, M., Yttri, K. E., Mihalopoulos, N., Kouvarakis, G., Beddows, D., Harrison, R. M., Cavalli, F., Putaud, J. P., Spindler, G., Wiedensohler, A., Alastuey, A., Pandolfi, M., Sellegri, K., Swietlicki, E., Jaffrezo, J. L., Baltensperger, U., and Laj, P.: A European aerosol phenomenology-5: Climatology of black carbon optical properties at 9 regional background sites across Europe, Atmos. Environ., 145, 346–364, https://doi.org/10.1016/j.atmosenv.2016.09.035, 2016.